The Light Stable Isotope (Hydrogen, Boron, Carbon, Nitrogen, Oxygen, Silicon, Sulfur) Composition of Orogenic Gold Deposits

Benoît Quesnel, Christophe Scheffer, and Georges Beaudoin

Abstract

Orogenic gold deposits formed in various terranes of most ages since the Paleoarchean and generally consist of quartz veins hosted in shear zones formed at the ductile brittle transition under greenschist to lower amphibolite metamorphic conditions. Vein mineralogy is dominated by quartz with various amounts of silicates, carbonates, phyllosilicates, borates, tungstates, sulfides, and oxides. The isotopic composition of these minerals and fluid inclusions has been investigated since the 1960s to constrain the characteristics of orogenic fluid systems involved in the formation of gold deposits worldwide. This review is based on 8580 stable isotope analyses, including $\delta^{18}O$, δD, $\delta^{13}C$, $\delta^{34}S$ $\delta^{15}N$, $\delta^{11}B$, and $\delta^{30}Si$ values, from 5478 samples from 558 orogenic gold deposits reported in the literature from 1960 to 2010. This contribution describes the variability of the light stable isotopic systems as function of the minerals, the age of the deposits, their regional setting, and their country rocks. The temperature of isotopic equilibrium of orogenic gold veins is estimated from mineral pairs for oxygen and sulfur isotopes. Based on these temperatures, and on fractionation between mineral and fluid components (H_2O, CO_2 and H_2S), the isotopic composition of fluids is estimated to better constrain the main parameters shared by most of auriferous orogenic fluid systems. Orogenic gold deposits display similar isotopic features through time, suggesting that fluid conditions and sources leading to the formation of orogenic gold deposits did not change significantly from the Archean to the Cenozoic. No consistent secular variations of mineral isotope composition for oxygen ($-8.1‰ \leq \delta^{18}O$ 33‰, n = 4011), hydrogen ($-187‰ \leq \delta D$ −4‰, n = 246), carbon ($-26.7‰ \leq \delta^{13}C$ 12.3‰, n = 1179), boron ($-21.6‰ \leq \delta^{11}B$ 9‰, n = 119), and silicon ($-0.5‰ \leq \delta^{30}Si$ 0.8‰, n = 33) are documented. Only nitrogen ($1.6‰ \leq \delta^{15}N \leq 23.7‰$, n = 258) and sulfide sulfur from deposits hosted in sedimentary rocks ($-27.2‰ \leq \delta^{34}S \leq 25‰$, n = 717) display secular variations. For nitrogen, the change in composition is interpreted to record the variation of $\delta^{15}N$ values of sediments devolatilized during metamorphism. For sulfur, secular variations reflect

Supplementary Information The online version contains supplementary material available at https://doi.org/10.1007/978-3-031-27897-6_10.

B. Quesnel · C. Scheffer · G. Beaudoin (✉)
Département de Géologie et Génie Géologique, Centre de recherche sur la géologie et l'ingénierie des ressources minérales (E4m), Université Laval, Québec G1V 0A6, Canada
e-mail: georges.beaudoin@ggl.ulaval.ca

D. Huston and J. Gutzmer (eds.), *Isotopes in Economic Geology, Metallogenesis and Exploration*, Mineral Resource Reviews, https://doi.org/10.1007/978-3-031-27897-6_10

incorporation of local sedimentary sulfur of ultimate seawater origin. No significant variation of temperature of vein formation is documented for orogenic gold deposits of different ages. Quartz-silicate, quartz-carbonate and sulfide-sulfide mineral pairs display consistent temperatures of 360 ± 76 °C (1σ; n = 332), in agreement with the more common greenschist facies hostrocks and fluid inclusion microthermometry. Fluid sources for orogenic gold deposits are complex but the isotopic systems (hydrogen, boron, carbon, nitrogen, oxygen, sulfur) are most consistent with contributions from metamorphic fluids released by devolatilization of igneous, volcano-sedimentary and/or sedimentary rocks. The contribution of magmatic water exsolved from magma during crystallization is not a necessary component, even if permissible in specific cases. Isotopic data arrays can be interpreted as the result of fluid mixing between a high T (~550 °C)—high $\delta^{18}O$ (~10‰)—low δD (~−60‰) deep-seated (metamorphic) fluid reservoir and a low T (~200 °C)—low $\delta^{18}O$ (~2‰)—high δD (~0‰) upper crustal fluid reservoir in a number of orogenic gold deposits. The origin of the upper crustal fluid is most likely sea- or meteoric water filling the host rock porosity, with a long history of water–rock isotope exchange. Mixing of deep-seated and upper crustal fluids also explains the large variation of tourmaline $\delta^{11}B$ values from orogenic gold veins. Regional spatial variations of oxygen and hydrogen isotope compositions of deep-seated fluid reservoirs are documented between orogenic gold districts. This is the case for the Val-d'Or (Abitibi), Coolgardie and Kalgoorlie (Yilgarn) where the oxygen isotope composition of the deep-seated fluid end-member is 4‰ lower compared to that from the Timmins, Larder Lake, and Kirkland Lake districts (Abitibi). However, both mixing trends converge towards a common, low $\delta^{18}O$ upper crustal fluid end-member. Such variations cannot be related to fluid buffering at the site of deposition and suggest provinciality of the fluid source. The contribution of meteoric water is mainly recorded by fluid inclusions from Mesozoic and Cenozoic age deposits, but micas are not systematically in isotopic equilibrium with fluid inclusions trapped in quartz from the same vein. This suggests late involvement of meteoric water unrelated to deposit formation. Yet, a number of deposits with low δD mica may record infiltration of meteoric water in orogenic gold deposits. Isotope exchange between mineralizing fluid and country rocks is documented for oxygen, carbon, sulfur and silicon isotopes. Large variations (> 10‰) of sulfide $\delta^{34}S$ values at the deposit scale are likely related to evolving redox conditions of the mineralizing fluid during reaction with country rocks. Deposits hosted in sedimentary rocks show a shift to higher $\delta^{18}O$ values as a result of fluid/rock oxygen exchange with the regional sedimentary country rocks.

Keywords

Stable isotope · fractionation · temperature · fluid source · metamorphic crustal · hydrogen · oxygen · boron · carbon · nitrogen · sulfur · silicon

1 Introduction

Orogenic gold deposits comprise a diverse class of mineral deposits that contain the second largest resource of gold, after the Witwatersrand (Republic of South Africa) paleoplacers (Dubé and Gosselin 2007). In addition to their economic importance, orogenic gold deposits record important geological process active at mid-crustal levels, where the deformation behavior of rocks changes, with increasing depth, from brittle to ductile. The formation of orogenic gold deposits involves advection of significant volumes of crustal fluids, which carry large amounts of dissolved mass and energy at the scale of the crust.

The class of orogenic gold deposits was proposed by Groves et al. (1998) to combine gold deposits that shared numerous characteristics, yet had remained grouped under different deposit

types in literature. The orogenic gold deposits were defined to include a range of epigenetic gold styles variably named "mesothermal", "quartz-carbonate", "lode gold", "greenstone gold", "Mother Lode", "turbidite-hosted", "BIF (Banded-Iron Formation)-hosted", etc. The class of orogenic gold deposits was defined to include deposits where gold is the major economic metal, and which formed in volcanic and/or sedimentary, accretionary, metamorphic terranes in convergent settings of all ages. The geological characteristics of orogenic gold deposits have been reviewed by Goldfarb et al. (2005) and Goldfarb and Groves (2015) amongst others, and are briefly summarized hereafter. Orogenic gold deposits consist of gold-bearing quartz-carbonate veins or disseminated sulfides, commonly representing less than 5 vol.% sulfides, most commonly pyrite and arsenopyrite. The veins display a range of structural features from foliated shear bands to brittle breccia and are characteristically associated to steeply-dipping reverse faults, related to major crustal shear zones typically marking terrane boundaries. The country rocks are varied and include almost all types of volcanic, plutonic, sedimentary rocks and their metamorphosed equivalents. Hydrothermal alteration is characteristically narrow and controlled by the vein structures, replacing peak-metamorphic minerals by white mica, Fe–Mg carbonate minerals and sodic feldspar, being the most common. The veins formed from low-salinity (3–12 wt.% NaCl eq.) carbonic-aqueous hydrothermal fluids with $X_{CO_2} < 0.3$, at temperatures typically about 350 °C. Orogenic gold deposits formed at depths of less than 20 km, typically near the base of the seismogenic continental crust, under high, to supra-lithostatic, fluctuating fluid pressure. Deposits formed deeper in the crust are characterized by ductile deformation, with gold mineralization mostly in disseminated sulfide minerals or less commonly in foliated veins, and formed at the higher temperature range. Those formed higher in the crust are characterized by more brittle structures, and a lower temperature of formation.

In spite of these well-defined geological characteristics, the origin of hydrothermal fluids that formed orogenic gold deposits remains controversial. Goldfarb and Groves (2015) reviewed sources for fluids in orogenic gold deposits, stating that the stable isotope composition of the minerals is inconsistent between deposits, and leads to equivocal interpretations about the source of fluids and dissolved components. This is particularly intriguing since the auriferous hydrothermal fluids are considered to have a well-defined composition that should enable determination of the source(s) of fluids. Goldfarb and Groves (2015) reiterated a long-held view that fluid-rock exchange, at the site of reaction, could mask part of the original isotopic signature (Ridley and Diamond 2000). If the association of the orogenic gold deposits with a major shear zone is a well-established fact, the role of the shear zone has been contested from being a deep-seated fluid channelling feature (e.g., McCuaig and Kerrich 1998) to a breach into a mid-crustal low permeability barrier (Beaudoin et al. 2006).

The first major compilation of oxygen, H, carbon, sulfur stable isotope data for Au–Ag deposits in metamorphic rocks, now defined largely as orogenic gold deposits, was undertaken by Kerrich (1987). This led to the concept of provinciality in the oxygen isotope composition of orogenic gold deposits, inferred to indicate large and uniform fluid source rock volumes, but different for each orogenic gold vein field (McCuaig and Kerrich 1998). High $\delta^{18}O$ values are characteristic of the auriferous fluids forming orogenic gold deposits, with a range of $\delta^{18}O_{H2O}$ values of 6 to 11‰ for Precambrian deposits (McCuaig and Kerrich 1998) and of 7 to 13‰ for Phanerozoic deposits (Bierlein and Crowe 2000), and as shown by the range of quartz $\delta^{18}O$ values of 6.9 to 25‰ for the 25 largest orogenic gold deposits (Goldfarb et al. 2005).

Goldfarb et al. (2005) compiled δD values ranging from −150 to −26‰ for mica and from −98 to −24‰ for fluid inclusions from the 25 largest orogenic gold deposits. Using the likely temperatures of isotopic equilibrium, the hydrothermal fluids δD values were suggested to range from −80 to −20‰, excluding low values from fluid inclusions of dubious or mixed origins

(McCuaig and Kerrich 1998; Goldfarb et al. 2005). Combined with the estimated fluid $\delta^{18}O$ values of 6 to 14‰, this has been taken as a strong indication for a metamorphic source for the auriferous fluids (McCuaig and Kerrich 1998).

The carbon isotope composition of hydrothermal carbonates associated with gold mineralization was shown to range mostly between −10 and 0‰, with outlier values as low as −32‰ (Goldfarb et al. 2005). McCuaig and Kerrich (1998) also remarked the narrow range in $\delta^{13}C$ values for a given deposit. The isotope composition of carbon has led to interpretation of a number of potential sources, from the mantle to magmas, to crustal devolatilization, mixing and redox reactions (McCuaig and Kerrich 1998). Likewise, the sulfur isotope composition of sulfides are summarized to mostly range from 0 to 9‰, but with a total range from −20 to 25‰, interpreted to reflect local sulfur sources (Goldfarb et al. 2005).

Despite the low variance in geological features, and in the chemical PVTX characteristics of auriferous fluids associated with orogenic gold deposits, the variation of the stable isotope composition of hydrothermal minerals and fluid inclusions has led to various, at times conflicting or equivocal, interpretations. Here, we attempt to address the variations in the stable isotope composition of hydrothermal minerals and fluid inclusions in orogenic gold deposits on the basis of a detailed analysis of an extensive compilation of data published between 1960 and 2010. The study of the database allows to outline major stable isotope compositional features for orogenic gold deposits to yield improved understanding of the sources of fluids, carbon, sulfur, nitrogen, boron and silicon for this deposit type.

2 Methodology

2.1 Database

The database integrates fifty years of stable isotope and orogenic gold deposit research published between 1960 and 2010, since which time data interpretation has been ongoing (Beaudoin 2011). Review of data published since 2010 shows no special features from more recent studies, but specific cases are discussed in relation to pre-2010 data. The first study of stable isotopes in orogenic gold systems was on the sulfur isotope composition of gold quartz veins of the Yellowknife district, Canada (Wanless et al. 1960). Because gold-bearing quartz ± carbonate veins have been described using a range of descriptive names from lode to quartz-carbonate to orogenic gold veins, the search in literature has used all known terms used to identify stable isotope research for this deposit type. The deposits compiled in the database comprise all the major orogenic gold deposits as defined by Goldfarb et al. (2005). Some of the deposits aggregated in the compilation have controversial metallogenic affinity. Nevertheless, the amount of data from deposits of controversial metallogenic affinity is small, such that it should not significantly impact on the overall stable isotope characteristics of orogenic gold deposits, unless otherwise noted. Data were compiled from 193 references, for which tabulated stable isotope values were reported (Supplementary Material Spreadsheet 1). Data reported in figures or as range of values, without individual mineral composition, were not considered in this study. The data were compiled dominantly from peer-reviewed journals, with the exception of a few major deposits for which data were only available in university theses.

The database contains 8580 stable isotope analyses for oxygen (n = 4014), hydrogen (n = 706), carbon (n = 1244), sulfur (n = 2215), nitrogen (n = 254), boron (n = 117) and silicon (n = 30) from 5478 samples (Supplementary Material Spreadsheet 1). Stable isotopic compositions are expressed in ‰, and are reported relative to VSMOW, VPDB, VCDT, AIR, NIST SRM 951, and NBS28 for $\delta^{18}O$ and δD, $\delta^{13}C$, $\delta^{34}S$, $\delta^{15}N$, $\delta^{11}B$ and $\delta^{30}Si$, respectively. Data reported in literature relative to SMOW, PDB and CDT are considered identical to the newer IAEA Vienna (V-) standards. Where samples have the same name, and several isotope or mineral analyses are reported, the results are deemed to be from the same sample even though textural equilibrium can seldom be verified.

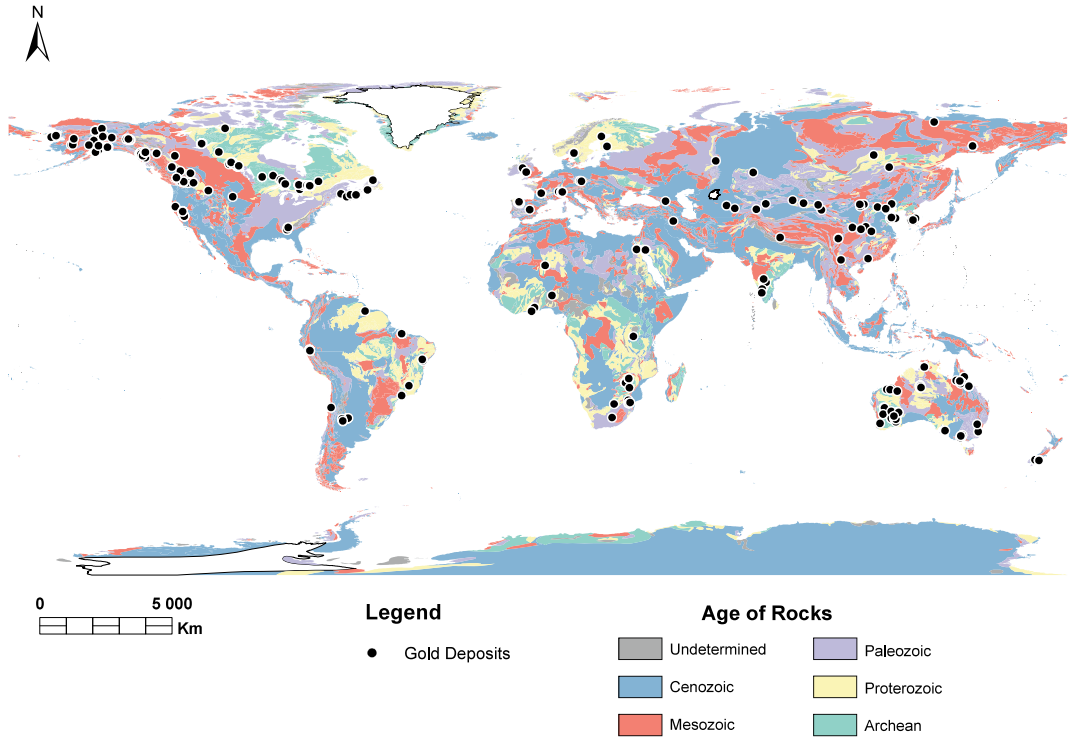

Fig. 1 Location of orogenic gold deposits with stable isotope data. The world geology map is prepared using digital data from Gosselin and Dubé (2005)

Oxygen isotope compositions have been measured in 22 minerals. Two studies report $\delta^{18}O$ values from fluid inclusions (FI) hosted by quartz or scheelite (Santosh et al. 1995; Billstrom et al. 2009), which are not considered further because the $\delta^{18}O$ values are most likely equilibrated with the host mineral oxygen. The hydrogen isotope composition has been measured in seven minerals and from FI in quartz. Mao et al. (2008) report seven δD values from "K-feldspar". Because the source of hydrogen in theses analyses is unspecified, but likely to be from FI, these data were not included in the database. Carbon isotopic compositions have been measured in seven minerals and in FI trapped in quartz and scheelite. Sulfur isotopic compositions have been measured in 13 minerals. Nitrogen and silicon isotopic composition have been measured in three and two minerals, respectively. Boron has been measured in tourmaline. The samples are from 564 deposits from all continents with the exception of Antarctica (Fig. 1), and range in age from the Archean to the Cenozoic, including 180 Archean, 68 Proterozoic, 104 Paleozoic, 129 Mesozoic, and 83 Cenozoic deposits. For Archean deposits, most of them are Neo-Archean (n = 164), with fewer Paleo- (n = 2) and Meso-Archean (n = 13). The age of the gold deposits is known with variable accuracy, such that geochronological data yield precise age for some deposits, whereas only age inferences can be made for others.

Gold deposits are hosted in a range of country rock types including sedimentary, volcano-sedimentary, or igneous rocks with variable chemical composition from felsic to ultramafic. For deposits hosted by several types of rocks, the dominant lithology/chemical composition is recorded in the database. Sedimentary rock-hosted deposits include unmetamorphosed clastic and/or chemical sedimentary rocks (greywackes, sandstones, shales, limestones, mudstones, argilites, BIF) or their metamorphosed equivalents (paragneiss, schist) which are

all reported as "sedimentary" for simplicity. Volcano-sedimentary rock-hosted deposits are mainly represented by Archean and Proterozoic greenstone belts. Igneous rock-hosted deposits include plutonic or volcanic rocks. Volcanic rocks mainly consist of rhyolite to basaltic rocks in greenstone belts, as well as mafic and ultramafic dykes. Plutonic rocks include a wide variety of rocks such as tonalite-trondhjemite-granodiorite (TTG) batholiths as well as granitic—diorite intrusions in various geological environment. Based on the description provided in each publication, geochemical descriptors (felsic, intermediate, mafic and ultramafic) are used to summarize the composition of dominant intrusive and volcanic rocks.

Deposits associated with zeolite, prehnite-pumpellyite or sub-greenschists facies, and/or "low" metamorphic grade rocks, have been combined into a sub-greenschist category. Those hosted by lower, middle, or upper greenschist facies rocks have been classified into a greenschist category. Lower, middle, or upper amphibolite, and granulite metamorphic facies host rocks are categorized into a high-grade metamorphic category. The resulting categories must be used with caution since orogenic gold deposits commonly post-date regional metamorphism. Moreover, in numerous studies, the metamorphic grade is not accurately described or covers a range, such as "lower greenschist to amphibolite". In such cases, we arbitrarily attributed a deposit to the higher metamorphic grade. Finally, for most of deposits from the North China Craton, a metamorphic grade class is not attributed because the gold deposits formed during the Mesozoic, significantly younger than Precambrian regional granulite grade metamorphism.

2.2 Temperature of Equilibrium

There can be several isotopic fractionations for a pair of minerals (e.g. δ_{quartz}–$\delta_{mineral}$) (Beaudoin and Therrien 2009) such that the computed temperatures can vary depending on the selected fractionation. Oxygen isotope fractionations derived from previous studies by Vho et al. (2019) are used for temperature estimates from quartz-tourmaline, quartz-chlorite, quartz-biotite, quartz-muscovite, quartz-albite, quartz-plagioclase, quartz-feldspar, quartz-ankerite, quartz-calcite and quartz-dolomite mineral pairs and are reported with a 2σ confidence interval (Supplementary Material, Spreadsheet 2). For quartz-sericite,[1] no fractionation equation exists in literature and, consequently, we use the quartz-muscovite fractionation equation from Vho et al. (2019). For quartz-scheelite, only one fractionation equation is available (Zheng 1992), but it yields low temperatures (mainly between 110 and 200 °C), inconsistent with the greenschist facies conditions and other geothermometers. Consequently, a combination of two equations, quartz-H_2O from Clayton et al. (1972) and scheelite-H_2O from Wesolowski and Ohmoto (1986), has been used to estimate the temperature of equilibrium between quartz and scheelite.

For quartz-plagioclase, quartz-feldspar and quartz-carbonate pairs, no information about the composition of the mineral is provided. Consequently, data are not presented in δ_{quartz}–$\delta_{mineral}$ diagrams and temperatures have not been calculated.

For sulfide pairs, pyrite-galena, pyrite-chalcopyrite, pyrite-pyrrothite, pyrite-sphalerite, sphalerite-chalcopyrite and chalcopyrite-galena fractionation data are from Kajiwara and Krouse (1971). The fractionation from Liu et al. (2015) was used for sphalerite-galena. The data are plotted in $\delta_{mineral}$–$\delta_{mineral}$ diagrams overlain by isotherms ranging from 250 to 550 °C.

2.3 Oxygen and Hydrogen Isotope Composition of Water

Oxygen and hydrogen isotope compositions of H_2O are calculated from quartz and OH-bearing minerals pairs that yield equilibrium

[1] We use "sericite" herein as a general term for unspecified white mica, as this term is used in the cited reference, even though the term has been disapproved by the International Mineralogical Association. In most cases "sericite" refers to fined grained muscovite, phengite or related white micas.

temperatures in the range 250–550 °C. This temperature range is consistent with the accepted range in temperature of formation for orogenic gold deposits (Goldfarb and Groves 2015). Thus, it is presumed that those mineral pairs record O–H isotope equilibrium. The water isotopic composition has been calculated using various hydrogen mineral-H_2O fractionations and oxygen quartz-H_2O fractionation equation from Vho et al. (2019). The entire dataset is presented in Supplementary Material 2. For tourmaline and chlorite, the fractionations of Kotzer et al. (1993) and Graham et al. (1984) have been used, respectively. For biotite and muscovite (or sericite) the hydrogen fractionations from Suzuoki and Epstein (1976) were used.

2.4 Carbon Isotope Composition of CO_2

The carbon isotope composition of CO_2 was calculated using calcite-CO_2 and dolomite-CO_2 fractionations from Ohmoto and Rye (1979) assuming equilibrium temperatures in the range 250–550 °C as determined from quartz-calcite and quartz-dolomite oxygen fractionation data (Vho et al. 2019). Because there are no carbon ankerite-CO_2 fractionation in literature, we did not compute $\delta^{13}C$ of CO_2 from ankerite. The entire dataset is presented in Supplementary Material 2.

3 Stable Isotope Composition of Minerals and Fluid Inclusions

3.1 Oxygen Isotopes

3.1.1 Silicates, Tungstates, Borates and Oxides

The oxygen isotope composition of 2357 quartz samples from orogenic gold deposits ranges from 5.2 to 25.9‰ (Fig. 2). Quartz $\delta^{18}O$ values show a broad, bimodal, distribution with one mode near 11.5‰, and the second near 15‰ (Fig. 2).[2] Quartz from orogenic gold deposits formed during the Archean shows this bimodal distribution, whereas quartz from deposits formed during the Proterozoic are characterized by $\delta^{18}O$ values about the lower mode (11.6‰; Fig. 2a). Orogenic gold deposits formed during the Phanerozoic have quartz $\delta^{18}O$ values about the higher mode (15‰) and tailing towards the highest $\delta^{18}O$ values (Fig. 2a).

Figure 2b shows the distribution of quartz $\delta^{18}O$ values for orogenic terranes for which there is more than 50 analyses. Quartz from the Archean Yilgarn Craton (Australia) shows a normal distribution about the 11.5‰ mode, with few higher values. In contrast, quartz from the Archean Superior Craton (Canada) displays a bimodal distribution. Quartz from the Proterozoic Trans-Hudson Orogen (Canada) plots mostly about the 11.5‰ mode. Quartz from the Appalachian/Caledonian and Hercynian orogens (America and Europe) plots mostly near 13.5‰ whereas those from the Tasman Orogen (Australia) are characterized by higher values with a mode near 16.5‰. Mesozoic and Cenozoic orogenic gold deposits from the Cordillera (North America) are characterized by heavier quartz oxygen isotope compositions mainly between 12.5‰ and 19.5‰ (Fig. 2b). Mesozoic orogenic gold deposits from the Daebo Orogen and North China Craton (China, Korea) plot mostly near 13‰.

Figure 2c shows the distribution of all quartz $\delta^{18}O$ values as function of the principal country rock type. Quartz hosted in igneous rocks shows the lowest $\delta^{18}O$ values with a normal distribution centered at 11.5‰. Deposits hosted in sedimentary country rocks have higher $\delta^{18}O$ values with a normal distribution centered at 15‰. The $\delta^{18}O$ values for deposits hosted in volcano-sedimentary rocks display a bimodal distribution with modes centered at 12‰ and 15‰. Most of the high $\delta^{18}O$ values are from deposits hosted by sedimentary and volcano-sedimentary rocks. The distribution of $\delta^{18}O$ values for quartz hosted in igneous rocks, divided by geochemical affinity, is presented on

[2] The character (uni-, bi- or polymodal) of the distribution and the location of the modes were determined visually. Modes refer to the class with the most observations.

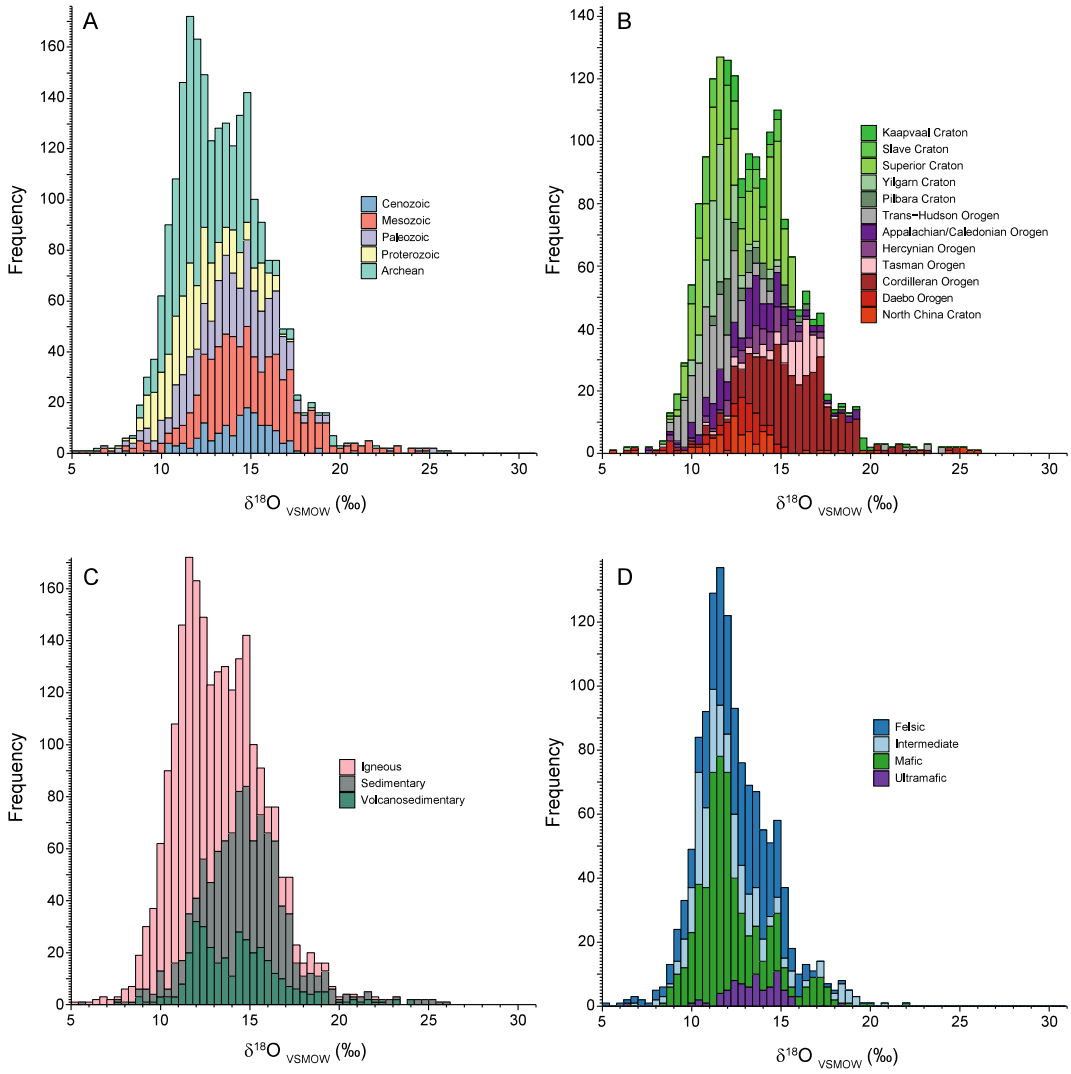

Fig. 2 Histograms showing $\delta^{18}O$ values of quartz forming veins from orogenic gold deposits based on: **a** the age of deposits; **b** the craton or orogen hosting the deposits (only craton or orogen with more than 50 $\delta^{18}O$ values are shown); **c** country rock of deposits; and **d** the geochemistry of igneous rocks hosting the deposits

Fig. 2d. No major difference is identified between mafic and felsic country rocks, both showing a unimodal distribution about the major 11.5‰ mode. Vein quartz hosted in ultramafic rocks ranges between 11.5‰ and 15.5‰, without a well-defined mode.

Quartz from orogenic gold districts from the Archean Superior Craton displays distinct oxygen isotopic compositions. The lower $\delta^{18}O$ values, between 9‰ and 14‰, with a mode centered on 11‰ are characteristic of the Val-d'Or district, whereas the higher $\delta^{18}O$ values between 13‰ and 16‰, with a mode at 15‰ are mostly from the Timmins district (Fig. 3a). There is no grouping of $\delta^{18}O$ values for other districts perhaps because of the smaller number of analyses. The difference in $\delta^{18}O$ values between the Val-d'Or and the Timmins districts correlates with the distribution of $\delta^{18}O$ values as function of the type of country rocks (Figs. 3a, b). Quartz from veins hosted in igneous rocks have $\delta^{18}O$ values ranging from 5 to 22‰ with a main mode

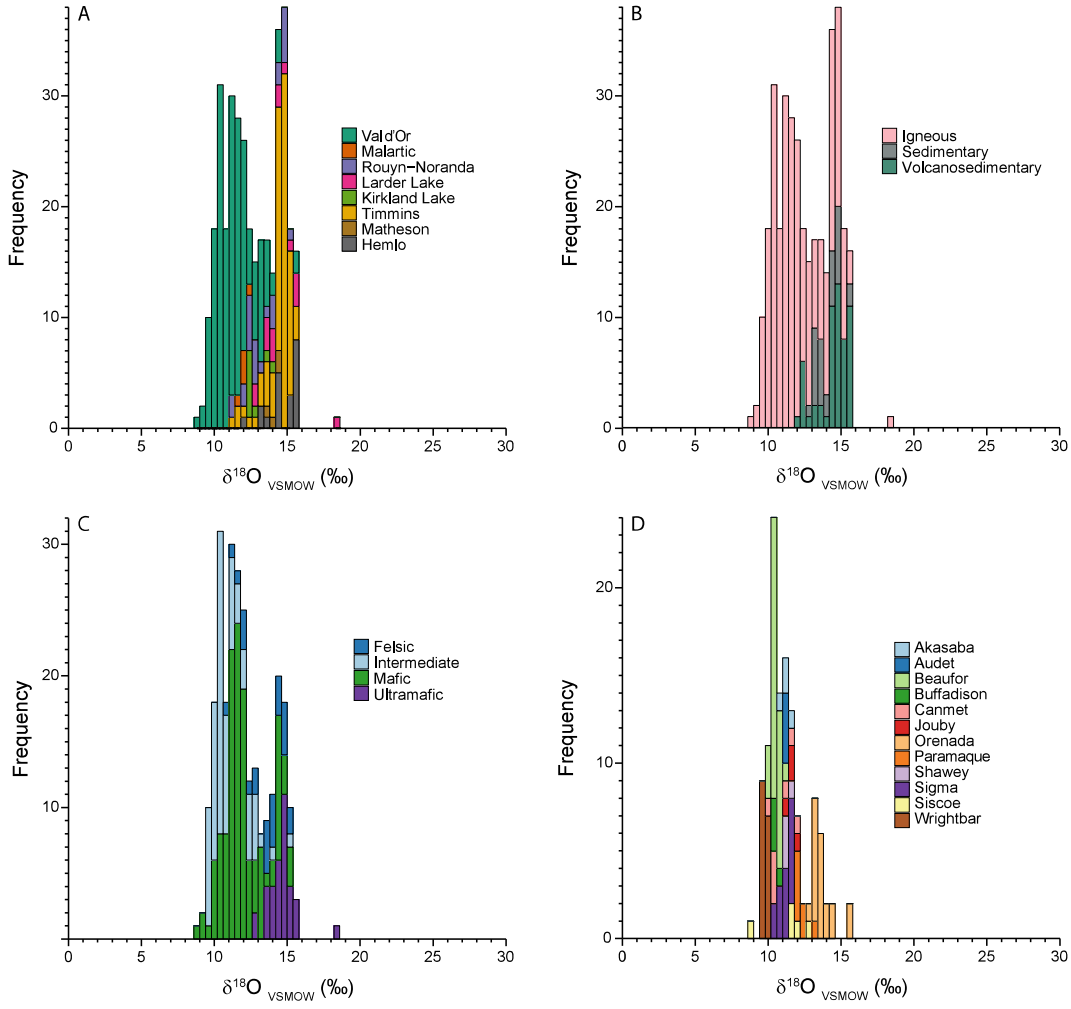

Fig. 3 Histograms showing $\delta^{18}O$ values of quartz forming veins from orogenic gold deposits from the Superior Craton based on: **a** district; **b** country rocks; **c** geochemistry of igneous rocks hosting deposits; and **d** deposits from the Val-d'Or district

at 11‰, whereas those hosted in sedimentary displays higher $\delta^{18}O$ values, between 5 and 27‰, with a mode at 14.5‰, and those hosted in volcano-sedimentary rocks have values between 7 and 24‰, with modes at 11.5 and 14.5‰. As shown in Fig. 3c, the igneous rocks hosting deposits with high quartz $\delta^{18}O$ values are mainly ultramafic.

For the Yilgarn Craton, quartz $\delta^{18}O$ values range mainly between ~10 and ~14‰, with no distinction between districts (Fig. 4a). Most of these veins are hosted in mafic igneous rocks and the few hosted in volcano-sedimentary rocks have similar $\delta^{18}O$ values (Figs. 4b, c). In districts from the Cordilleran Orogen for which there are more than 20 analyses, quartz displays $\delta^{18}O$ values mostly between ~12 and ~20‰ (Fig. 4d) higher than those documented from the Superior and Yilgarn cratons. In the Cordilleran Orogen, the Fairview, Klondike and Bridge River districts (12–14‰, 14–16‰ and 18–20‰, respectively) in Canada, the Berners Bay (12 to 16‰) and Mother Lode districts (16–19‰; United States of America—USA) display distinct ranges of $\delta^{18}O$ values. In contrast, the $\delta^{18}O$ values from the Nome district (USA) define a

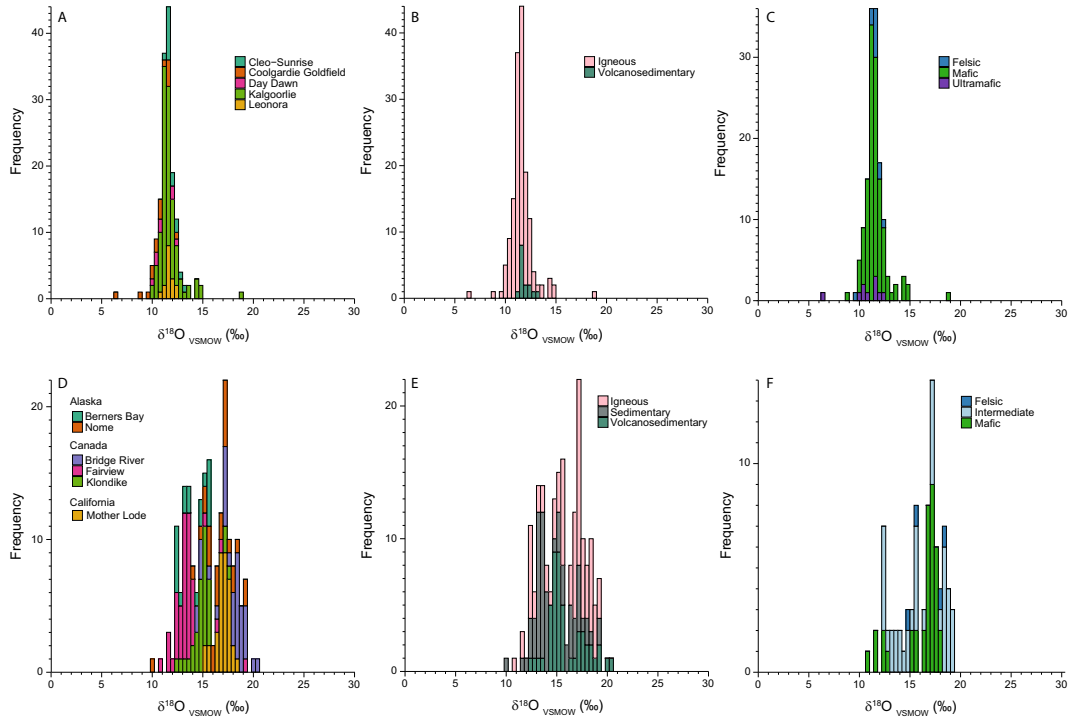

Fig. 4 Histograms showing $\delta^{18}O$ values of quartz forming veins from orogenic gold deposits from the Yilgarn Craton and Cordilleran Orogen based on: **a** district (Yilgarn Craton); **b** country rocks (Yilgarn Craton); **c** geochemistry of igneous rocks hosting deposits (Yilgarn Craton); **d** districts (Cordilleran Orogen); **e** country rocks (Cordilleran Orogen); and **f** geochemistry of igneous rocks hosting deposits (Cordilleran Orogen)

large range of values (10 to 20‰). All these districts are hosted in volcano-sedimentary and sedimentary rocks but in some of the districts, major deposits are hosted by granite (Fig. 4e). Data do not vary with the chemistry of the igneous rocks (Fig. 4f).

At the district scale, quartz from orogenic gold deposits is characterized by narrow ranges of $\delta^{18}O$ values (Fig. 3d). For example, in the Val-d'Or vein field, quartz from the Beaufor deposit is characterized by quartz oxygen isotope compositions in the range 9.9–11.1‰, with an average of 10.6 ± 0.2‰ (Beaudoin and Pitre 2005). Few studies allow comparison of several deposits in one district. In the Val-d'Or vein field, Beaudoin and Pitre (2005) and Beaudoin and Chiaradia (2016) showed no systematic variation in composition across vein thickness, along strike, or down-dip. In Val-d'Or, there is a gradual change in the average composition of quartz of a deposit at the scale of the district (Beaudoin and Pitre 2005).

Figure 5 presents the oxygen isotope composition of other silicates, tungstate, borates and oxides. Muscovite (n = 84) and sericite (n = 70) have $\delta^{18}O$ values ranging from 7.0 to 17.0‰ and 6.6 to 16.0‰, respectively (Fig. 5a), with one muscovite having a low $\delta^{18}O$ value of 0.7‰. Chlorite (n = 87) and biotite (n = 45) have similar $\delta^{18}O$ values ranging from 1.0 to 12.0‰ and from 2.0 to 12.6‰, respectively. Two talc samples yield $\delta^{18}O$ values of 7.0 and 7.9‰ (Fig. 5a). Scheelite (n = 54) has a small range of $\delta^{18}O$ values from 2.0 to 6.6‰, whereas tourmaline (n = 40) displays a wider range of $\delta^{18}O$ values from 4.9 to 11.0‰ (Fig. 5b). Actinolite (n = 19) has $\delta^{18}O$ values from 5.0 to 11.5‰, whereas two epidote samples yield $\delta^{18}O$ values of 7.7 and 9.6‰ (Fig. 5b). Undifferentiated feldspar (n = 20) and plagioclase (n = 20) have $\delta^{18}O$

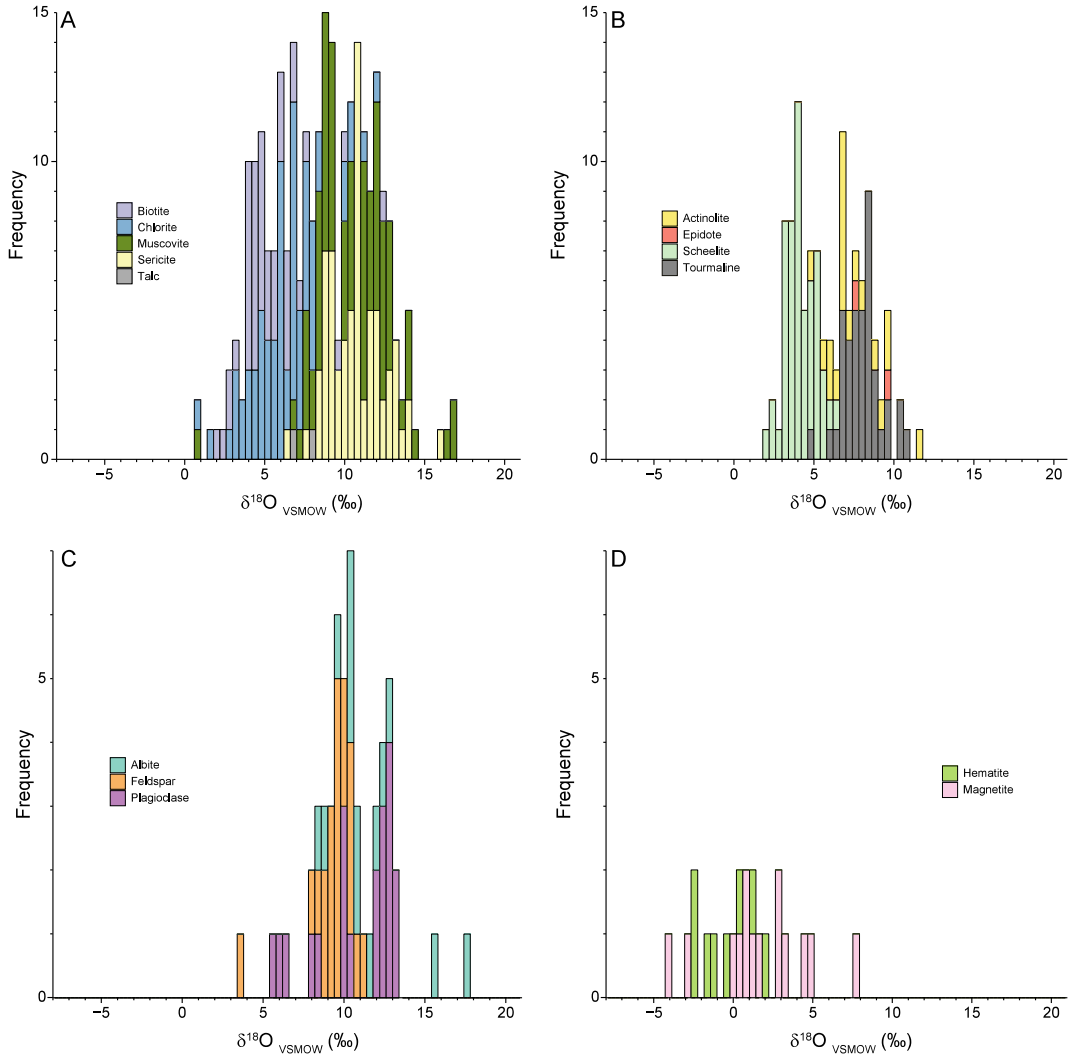

Fig. 5 Histograms showing $\delta^{18}O$ values of silicates and oxides minerals in deposits: **a** biotite, chlorite, muscovite, sericite and talc; **b** actinolite, epidote, scheelite, and tourmaline: **c** albite, feldspar and plagioclase; and **d** hematite and magnetite

values ranging from 3.6 to 11.3‰ and from 5.5 to 13.4‰, respectively, whereas albite (n = 17) displays $\delta^{18}O$ values from 8.3 to 17.8‰ (Fig. 5 c). Magnetite (n = 14) and hematite (n = 8) have low $\delta^{18}O$ values from −4.1 to 7.6‰ and from −2.3 to 2.2‰, respectively (Fig. 5d).

3.1.2 Carbonates

Figure 6 shows the oxygen isotope composition of carbonate minerals, including calcite (n = 493), dolomite (n = 345), ankerite (n = 207), siderite (n = 53), magnesite (n = 8) and undifferentiated carbonate minerals (n = 42). Carbonate $\delta^{18}O$ values show three modes, with two principal modes centered on 10‰ and 12.5‰ (Fig. 6a), and a third mode centered on 24‰. Ankerite, calcite and dolomite have $\delta^{18}O$ values ranging from 7.7 to 25.0‰, from 6.3 to 27.5‰, and from 1.2 to 25.3‰, respectively, with the same bimodal distribution for ankerite and calcite. Dolomite displays a bimodal distribution with two modes centered on 12‰ and 16‰. Siderite has $\delta^{18}O$

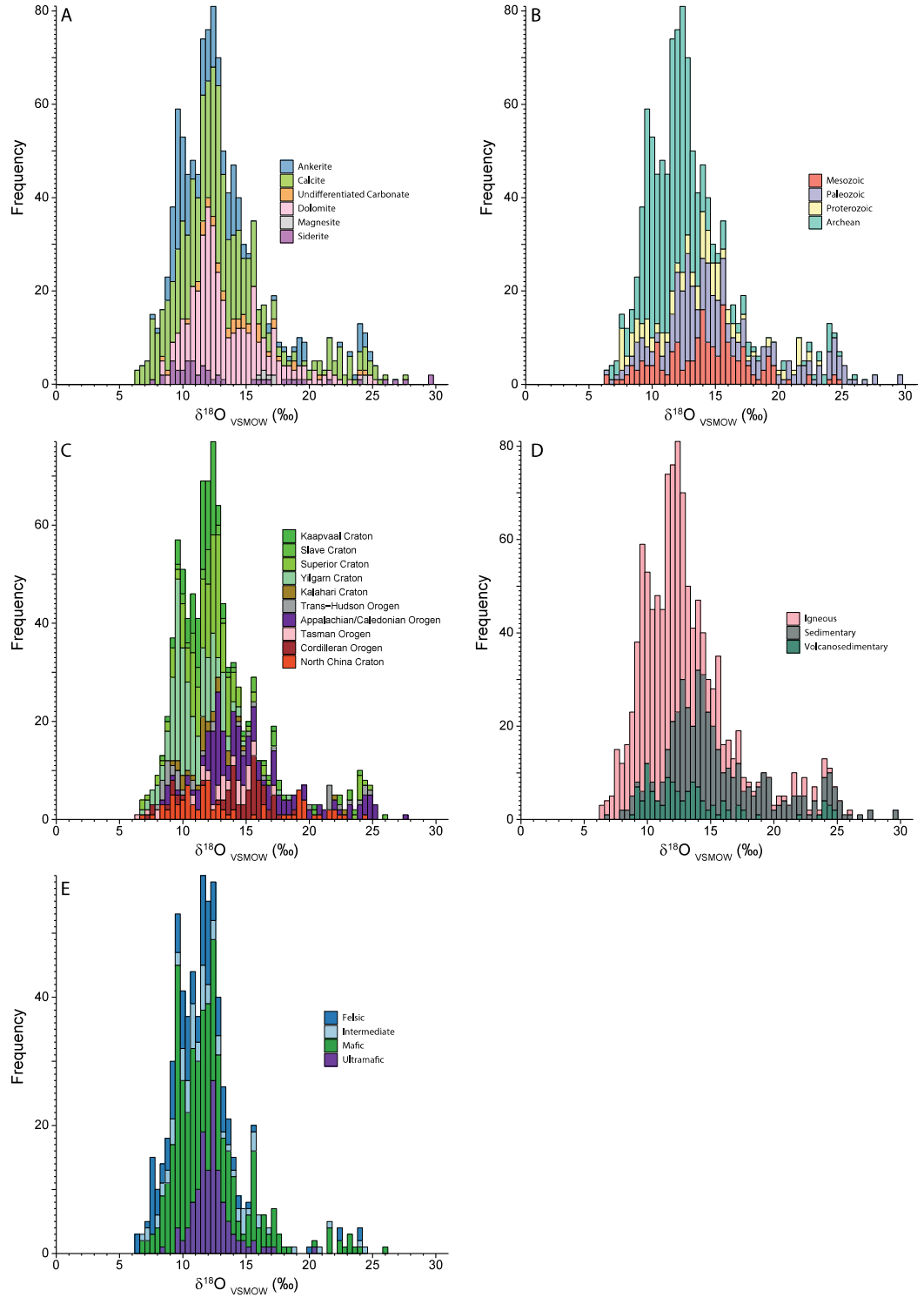

Fig. 6 Histograms showing $\delta^{18}O$ values of carbonate from veins in orogenic gold deposits according to: **a** carbonate mineral; **b** age of deposit; **c** craton or orogen hosting deposits (only craton or orogen with more than 30 $\delta^{18}O$ values are shown); **d** country rocks of deposits; and **e** geochemistry of igneous rocks hosting deposits

values ranging from 7.7 to 29.8‰, but most of data are around 11‰. The few $\delta^{18}O$ values of magnesite and undifferentiated carbonate minerals do not show consistent distribution patterns.

Archean deposits display a bimodal distribution of $\delta^{18}O$ values with two principal modes centered on 10‰ and 12.5‰ (Fig. 6b). Proterozoic deposits do not display a specific distribution of $\delta^{18}O$ values, whereas Paleozoic deposits display a bimodal distribution with two principal modes centered on 12.5‰ and 14.5‰. Mesozoic deposits have two main modes of $\delta^{18}O$ values at 14.5‰ and 16‰. Values higher than ~20‰, are mostly from Paleozoic deposits with only few Archean, Proterozoic and Mesozoic analyses. Figure 6c shows that $\delta^{18}O$ values for Archean cratons (Kaapvaal, Slave, Superior, Yilgarn) are mostly lower than ~15‰. The distribution of the $\delta^{18}O$ values from Yilgarn is centered on 10‰, whereas data from the Kaapvaal, Slave and Superior cratons are mostly centered on 12.5‰. For the Appalachian/Caledonian Orogen, $\delta^{18}O$ values are scattered about a large mode near 13‰. For others cratons/orogens, data are less numerous and scattered. Figure 6d displays carbonate $\delta^{18}O$ values as function of the country rock type. Deposits hosted in igneous rocks have a bimodal distribution with two modes about 10‰ and 12.5‰. Values for deposits hosted in sedimentary rocks display a normal distribution centered on ~14‰, whereas those hosted in volcano-sedimentary environment display three modes centered on ~10‰, ~12‰ and ~14‰. Figure 6e shows carbonate $\delta^{18}O$ values as function of the chemical composition of igneous country rocks. Deposits hosted in felsic to mafic rocks have two modes about 10‰ and 12.5‰. Deposits hosted in ultramafic rocks have a normal distribution of carbonate $\delta^{18}O$ values centered on 12.5‰.

3.1.3 Hydrogen Isotopes in Silicates

The hydrogen isotope composition (Fig. 7a) has been measured in muscovite (n = 86), sericite (n = 51), biotite (n = 32), chlorite (n = 42), actinolite (n = 9), epidote (n = 5), and tourmaline (n = 13). The range in δD values for vein minerals is remarkably wide, from −187 to −4‰ (Fig. 7a). The distribution of vein mineral δD values is bimodal, with a principal mode near -58‰, and a second mode near −85‰, with an asymmetric tail to low δD values. Epidote has the highest δD values (−30 to −4‰). Muscovite and sericite are characterized by δD values that spread mainly between −80 and −26‰, with a mode near −55‰, but with a wide spread to low δD values (−186‰; Fig. 7a). Chlorite displays a main mode at slightly lower values compared to muscovite and sericite (between −90‰ and −70‰), but also yields low δD values (−187‰). Biotite displays a relatively small range of δD values from −117 to −51‰ (Fig. 7a). Tourmaline and actinolite have δD values that span the range of the two main modes of hydrogen isotope compositions.

In Fig. 7b, δD values of minerals are reported relative to the age of the deposits. The bimodal distribution about the principal (−58‰) and the second (−85‰) modes encompasses δD values of all ages. However, Mesozoic and Cenozoic deposit δD values display a unimodal distribution centered around -58‰, with an asymmetric tail to the lowest δD values for deposits from the Cordillera Orogen. Deposits from Trans-Hudson Orogen display a unimodal distribution with values ranging between ~−120 and ~−30‰, and a mode at ~−90‰. For other cratons/orogens, data are less numerous and scattered.

Figures 7d and e show the distribution of δD values as function of country rock and of chemical composition of igneous rocks, respectively. No trends were identified, but the lowest values documented for Mesozoic and Cenozoic deposits from the Cordillera Orogen are from deposits hosted in sedimentary and volcano-sedimentary rocks.

3.1.4 Hydrogen Isotopes in Fluid Inclusions

Figure 8 presents the δD values of fluid inclusions extracted from quartz (n = 468). The range in δD values for fluid inclusions is from −179 to −7‰, with a wide and asymmetric distribution towards low δD values (Fig. 8a). The mode is centered on −70‰. Hydrogen isotope compositions of fluid inclusions from Archean,

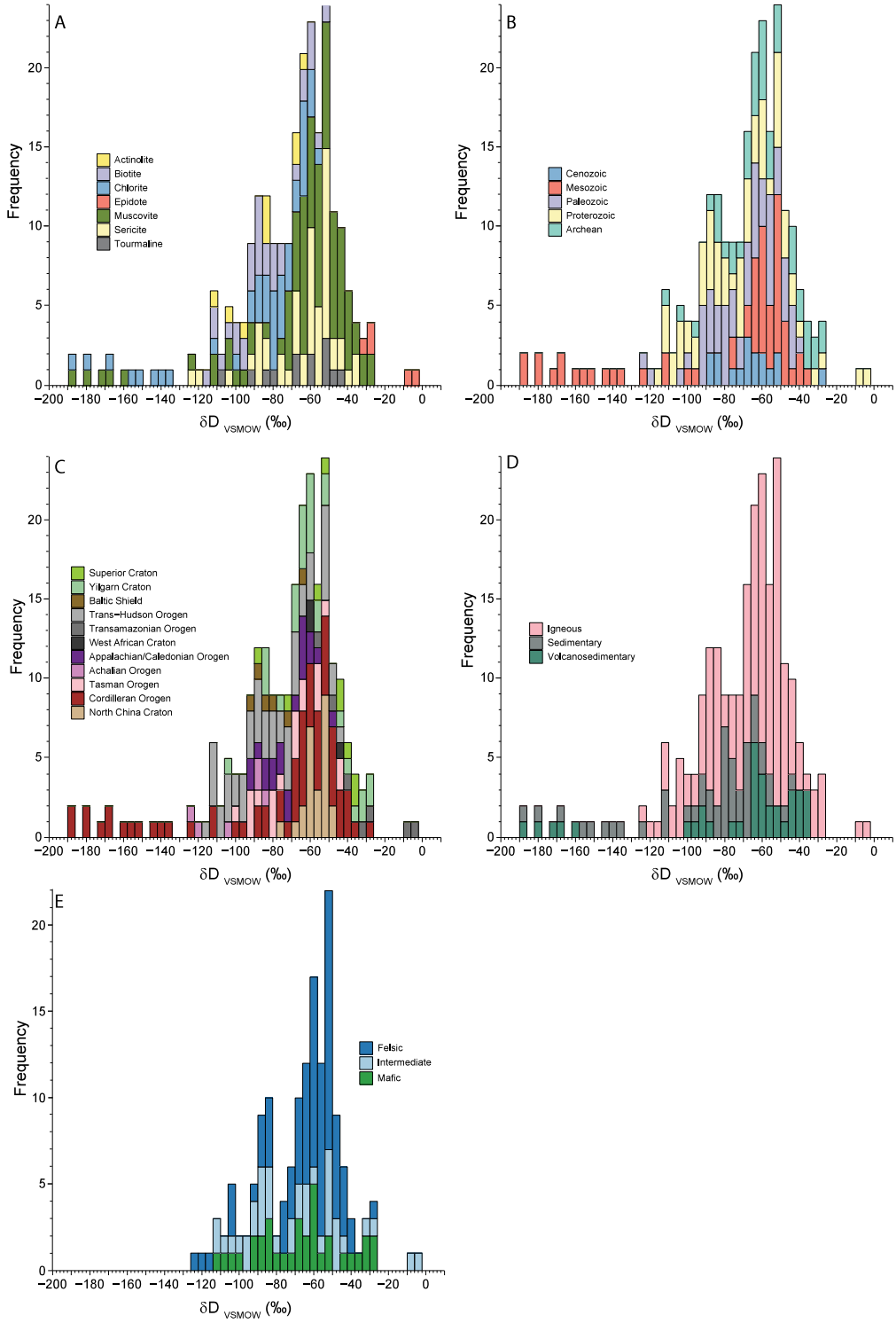

Fig. 7 Histograms showing δD values in OH-bearing minerals from veins from orogenic gold deposits based on: **a** nature of mineral; **b** age of deposit; **c** craton or orogen hosting deposits; **d** country rocks of deposits; and **e** geochemistry of igneous rocks hosting deposits

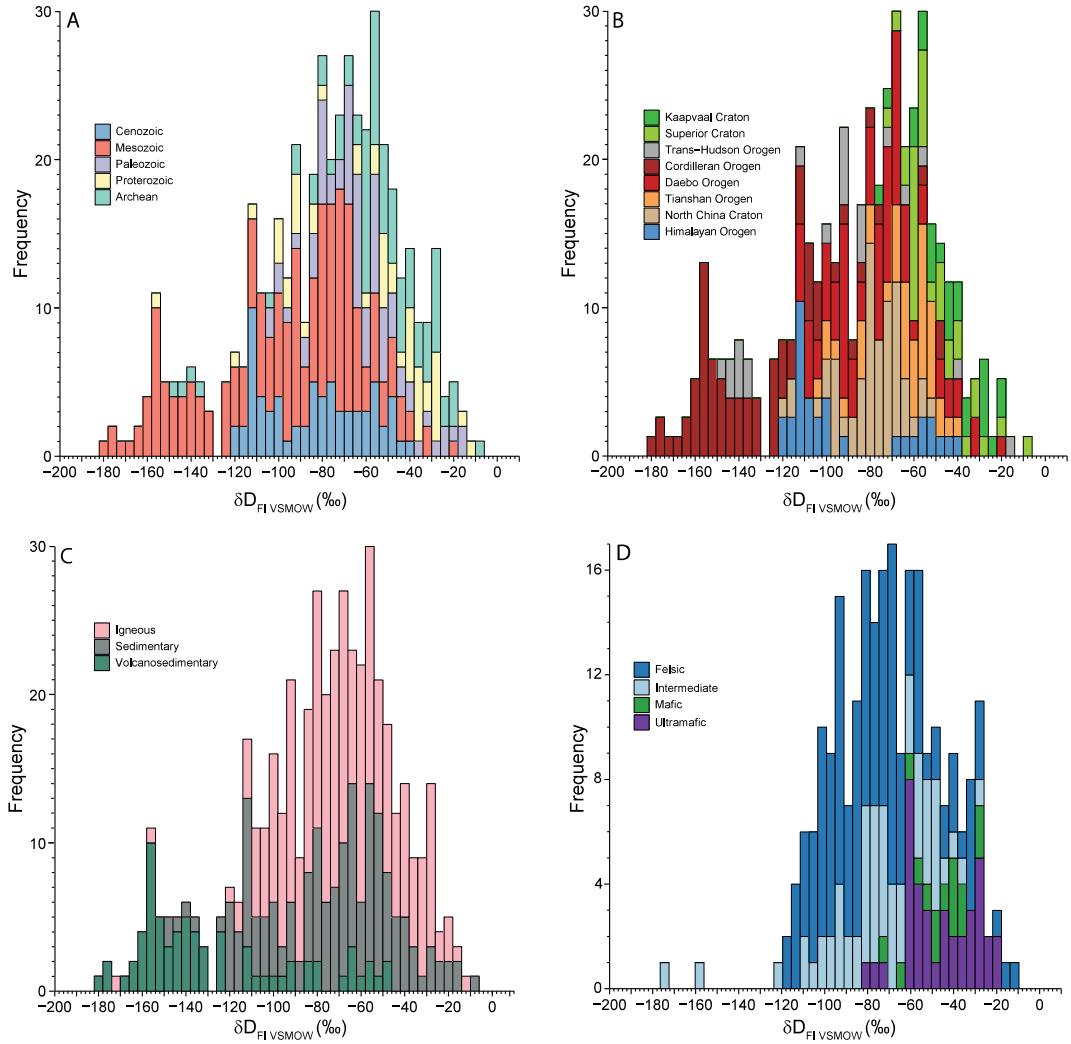

Fig. 8 Histograms showing δD values from fluid inclusion (FI) trapped in quartz from veins from orogenic gold deposits based on: **a** age of deposit; **b** craton or orogen hosting deposits (only craton or orogen with more than 20 δD values are shown); **c** country rocks of deposits; and **d** geochemistry of igneous rocks hosting deposits

Proterozoic, Paleozoic and Cenozoic orogenic gold deposits are typically heavier, from −7 to ∼−110‰, with few outlying values to ∼ −150‰ (Fig. 8a). Fluid inclusions δD values for Mesozoic orogenic gold deposits typically have values lower than −40‰, with a bimodal distribution with a mode near −70‰ and a second mode centered on −160‰ (Fig. 8a).

Figure 8b shows the distribution of δD values from fluid inclusions as function of craton/orogen. The main mode near −70‰ is dominated by deposits from the Daebo and Tianshan orogens, and from the North China Craton Craton. Deposits from the Himalayan Orogen display a wide range of δD values, with a secondary mode at ∼−110‰ from three deposits in Tibet (Supplementary material, Spreadsheet 1). The low δD values (< −120‰) are documented mainly for deposits hosted in the Cordillera Orogen, with a few measurements from deposits hosted in the Baltic Shield and the Trans-Hudson Orogen (Supplementary material, Spreadsheet 1).

Figure 8c shows δD values as function of the type of country rocks. The lowest δD values are

characteristic of volcano-sedimentary rocks hosting deposits in the Mesozoic Cordillera Orogen. The dominant country rocks of deposits with δD values higher than −120‰ are igneous and sedimentary with only few analyses for deposits hosted in volcano-sedimentary rocks. In Fig. 8d, δD values between −120‰ and −60‰ are mainly from deposits hosted by felsic to intermediate igneous country rocks, whereas mafic and ultramafic hosted deposits have fluid inclusions with δD values between −60‰ and −20‰.

3.1.5 Carbon Isotopes in Minerals and Fluid Inclusions

Figure 9a shows the distribution of the carbon isotopic compositions for calcite (n = 513), dolomite (n = 344), ankerite (n = 214), siderite (n = 44), magnesite (n = 7), undifferentiated carbonate minerals (n = 47), and graphite (n = 2). Most $\delta^{13}C$ values range from −15 to 3‰ with a wide mode at −4‰, a secondary mode around −14‰ and a third one at −22‰. The $\delta^{13}C$ values from fluid inclusions trapped in quartz and scheelite show a unimodal distribution centered near −6‰ with rare values as low as −26‰ (Fig. 10a).

There is no significant difference of $\delta^{13}C$ values as function of the mineral or fluid inclusions (Figs. 9a and 10a). In Archean deposits, carbonates have $\delta^{13}C$ between −8 and 3‰, whereas Proterozoic, Paleozoic and Mesozoic deposits have similar $\delta^{13}C$ values distributed from −15 to 3‰ with a mode at −5‰ (Fig. 9b). However, low $\delta^{13}C$ values are documented for Paleozoic deposits of the Meguma district hosted in sedimentary rocks (Appalachian/Caledonian Orogen; Fig. 9b, c, d).

Carbonates from Archean Slave, Superior, Kaapvaal and Yilgarn cratons and from the Mesozoic North China Craton Craton display $\delta^{13}C$ values between −7 and 0‰, whereas the range of $\delta^{13}C$ values from the West African Craton is centered on −13‰ (Fig. 9c).

The carbonate $\delta^{13}C$ values from deposits hosted by igneous rocks show a unimodal distribution with a mode near −4‰ (Fig. 9d). Volcano-sedimentary rock-hosted deposits display a narrow range of $\delta^{13}C$ values, between −10 and 0‰. Sedimentary rock hosted deposits show a multimodal distribution with a main mode at −6‰, and three other modes around −3, −13 and −22‰. Felsic igneous rocks hosted deposits show a unimodal distribution with a main mode at −4‰. The carbonate $\delta^{13}C$ values from deposits hosted in mafic and ultramafic rocks, mainly from −9 to 0‰, each show a distribution with a main mode near −3‰ (Fig. 9e).

3.1.6 Sulfur in Sulfides and Sulfates

The sulfur isotope composition of sulfides ranges from −30 to 17‰, with a mode at ∼ 3‰ and a tail to low $\delta^{34}S$ values. (Fig. 11a). Anhydrite (n = 3) and barite (n = 29) $\delta^{34}S$ values range from −2.9 to 18.2‰ with a mode at ∼8‰. Most $\delta^{34}S$ values are from pyrite (n = 1305), arsenopyrite (n = 258) and galena (n = 199). No variation of $\delta^{34}S$ in relation to sulfide species is identified. The $\delta^{34}S$ values are similar for deposits formed during the Archean and Proterozoic (Fig. 11b). However, Paleozoic age deposits show a bimodal distribution of $\delta^{34}S$ values with a main mode at 0‰ and a second mode at 3‰. Mesozoic and Cenozoic age deposits display a distribution of $\delta^{34}S$ values similar to that of Archean and Proterozoic deposits, although with a wider range to low and high $\delta^{34}S$ values.

The distribution of $\delta^{34}S$ values is homogeneous for all cratons/orogens, and most of the data are spread along the entire range as illustrated for the Slave, Superior and Daebo cratons/orogen (Fig. 11c). The range of $\delta^{34}S$ values from the West African Craton is narrower, from −12 to −5‰. However, these data are from six deposits and have been measured mainly on arsenopyrite (Fig. 11a). Similarly, the Trans-Hudson Orogen and Dharwar Craton display a narrow distribution from 2 to 10‰. No significant difference has been identified for $\delta^{34}S$ values from deposits hosted by igneous, sedimentary or volcano-sedimentary rocks (Fig. 11d). However, sulfide minerals from deposits hosted in sedimentary rocks display

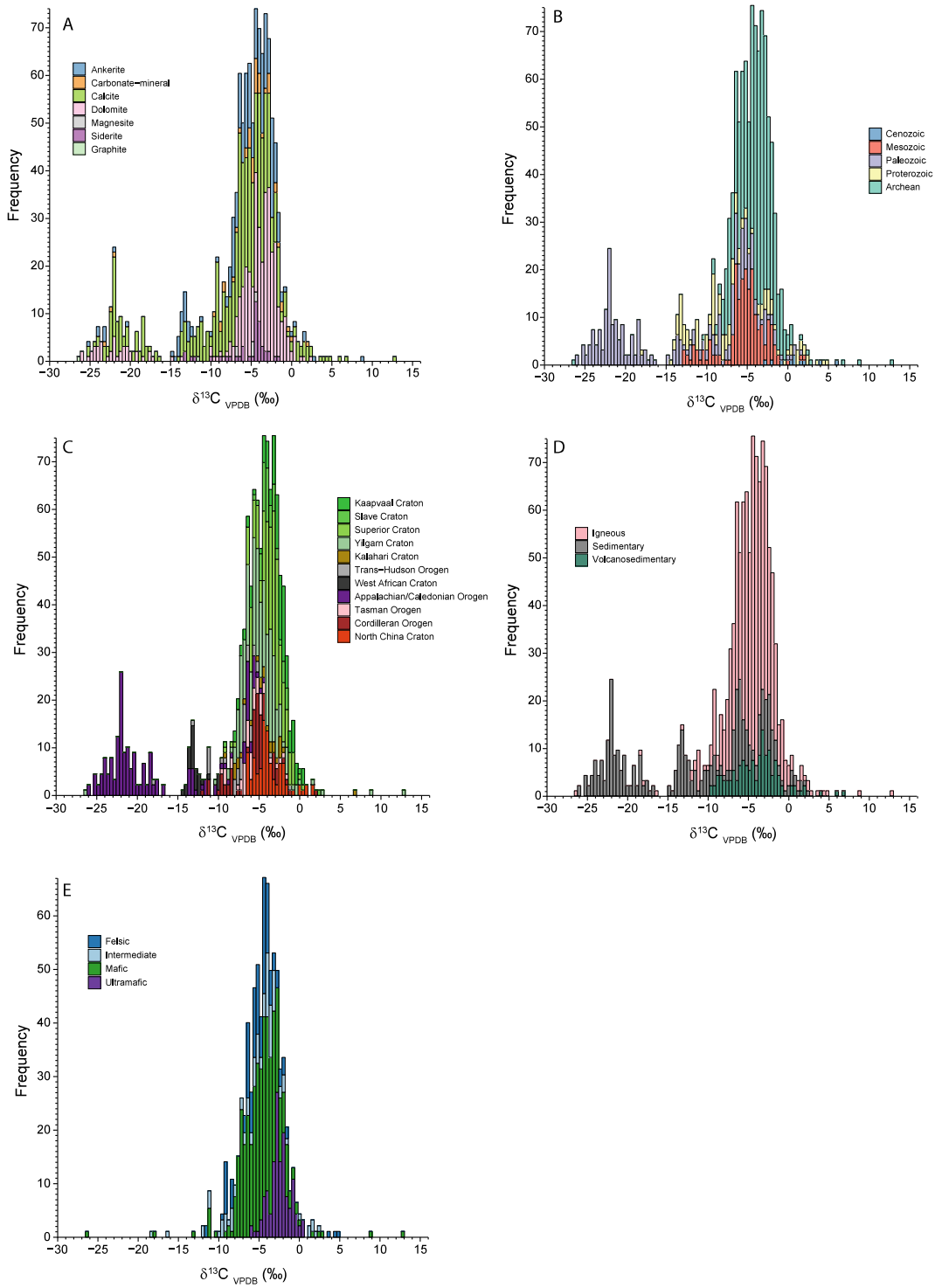

Fig. 9 Histograms showing $\delta^{13}C$ values of carbonate minerals and graphite from orogenic gold deposits based on: **a** nature of minerals; **b** age of deposit: **c** craton or orogen hosting deposits (only craton or orogen with more than 30 $\delta^{13}C$ values are shown); **d** country rocks of deposits; and **e** geochemistry of igneous rocks hosting deposits

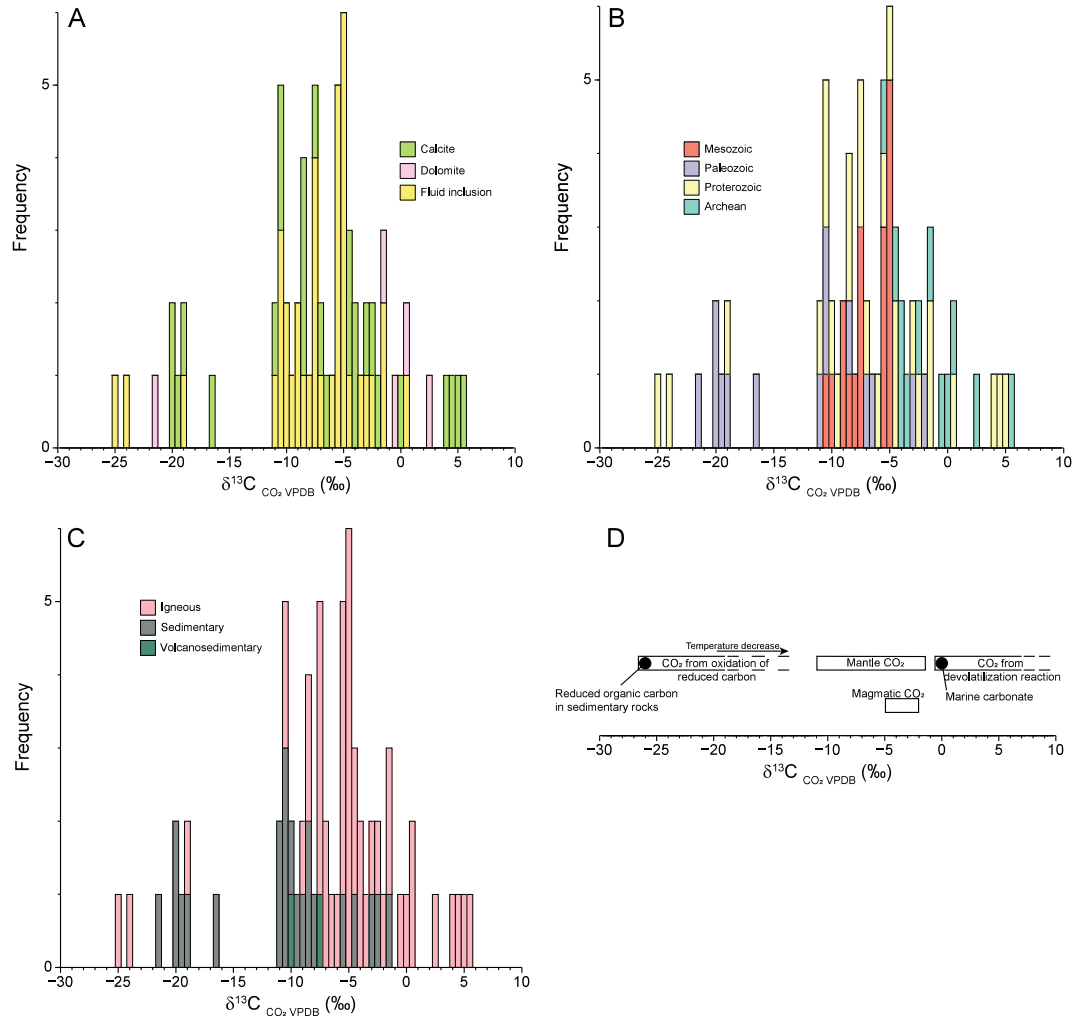

Fig. 10 $\delta^{13}C$ values of CO_2 from fluid inclusion (in quartz and scheelite) and CO_2 in equilibrium with calcite and dolomite using temperatures of equilibrium calculated using O isotope fractionation of Vho et al. (2019) on quartz-carbonate minerals pairs (see Fig. 13 and Supplementary material, spreadsheet 2). Histograms showing $\delta^{13}C_{CO_2}$ values are presented based on: **a** mineral; **b** age of deposit; and **c** country rocks of deposit. **d** shows $\delta^{13}C_{CO_2}$ values of various geological reservoirs (Taylor 1986; Kerrich 1989; Trull et al. 1993)

$\delta^{34}S$ variations with age (Fig. 11e). Archean deposits have $\delta^{34}S$ values with a unimodal distribution at 2.5‰, whereas Proterozoic deposits display a unimodal distribution at 4‰. Paleozoic deposits display a bimodal distribution with two main modes at 0‰ and 2.5‰ and with a number of values around 9‰. Mesozoic deposits display scattered $\delta^{34}S$ values with several data about 2.5‰ and tailing to low values. There are not enough data from Cenozoic age deposits to describe the distribution. The $\delta^{34}S$ values of minerals hosted by mafic to ultramafic igneous rocks show a bimodal distribution, with a main mode near 1.5‰ and a second mode at −5‰ (Fig. 11e). The range of $\delta^{34}S$ values for deposits hosted by felsic igneous rocks is slightly higher than for mafic rocks, between −5‰ and 15‰ with a mode at 3‰.

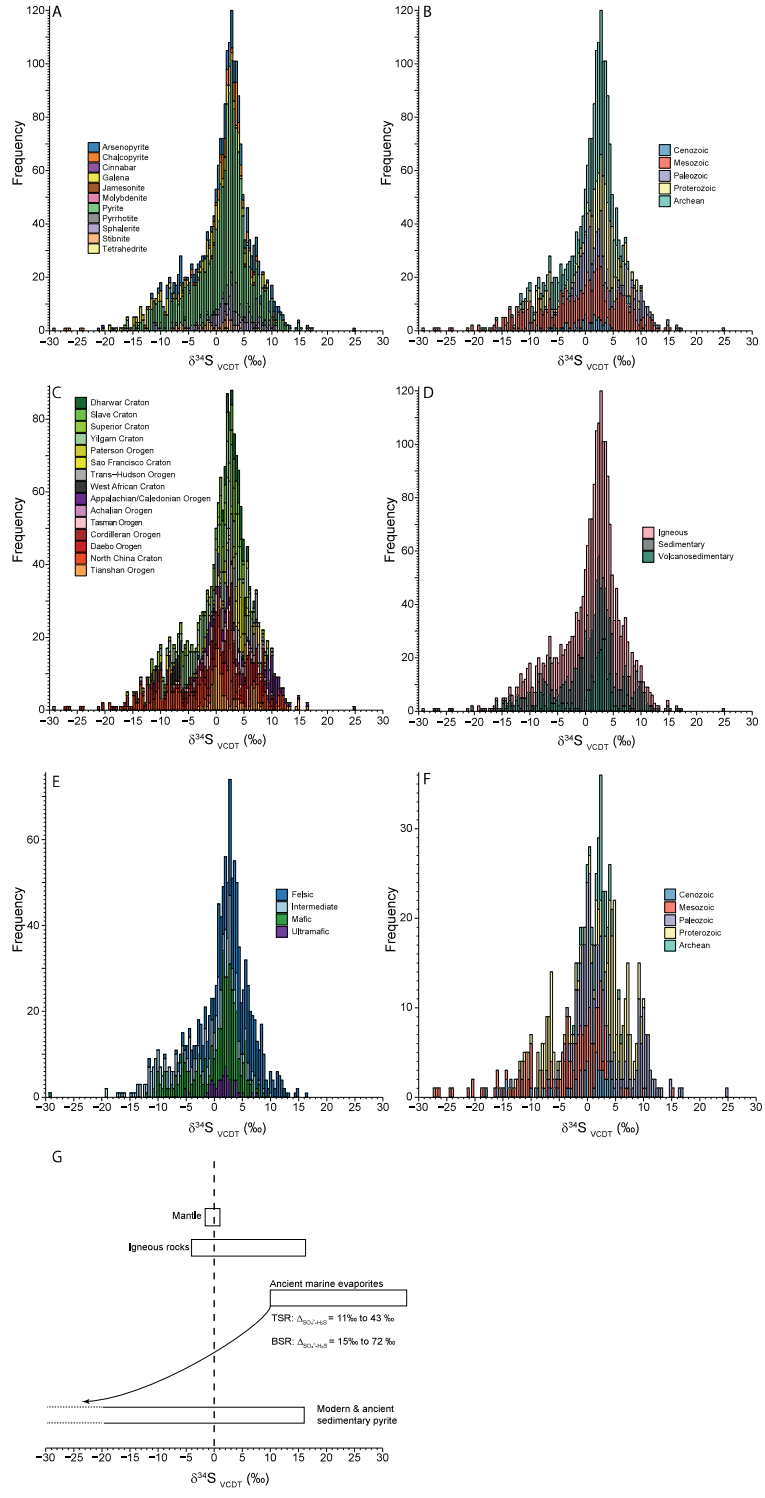

Fig. 11 Histograms showing $\delta^{34}S$ values of vein sulfide minerals from orogenic gold deposits based on: **a** mineral; **b** age of deposit; **c** craton or orogen hosting deposit (only craton or orogen with more than 50 $\delta^{34}S$ values are shown); **d** country rocks of deposits; **e** geochemistry of igneous rocks hosting deposits; and **f** age of deposits in sedimentary country rocks. **g** Variations in $\delta^{34}S$ values for various geological reservoirs (Machel et al. 1995; Wortmann et al. 2001; Seal 2006; Johnston et al. 2007; Labidi et al. 2013). $\Delta^{34}S^{2-}_{SO_4-H_2S}$ due to thermochemical sulfate reduction (TSR) calculateed at 500 °C and 100 °C (Eldridge et al. 2016)

3.1.7 Nitrogen in Silicates

The N isotope composition of biotite (n = 15), muscovite (n = 208) and K-feldspar (n = 31) range from 1 and 24‰ (Fig. 12a). Archean deposits have mostly $\delta^{15}N$ values higher than 10‰. Proterozoic deposits display a range between 7 to 12‰ whereas Phanerozoic deposits have mostly $\delta^{15}N$ values below 7‰ (Fig. 12b). Figure 12c shows that $\delta^{15}N$ values labelled by craton/orogen mimics the distribution as a function of the age of the deposits. Figure 12d shows that low $\delta^{15}N$ values are mostly documented from deposits hosted in volcano-sedimentary and sedimentary rocks whereas higher values are mainly from igneous rock hosted deposits.

3.1.8 Boron in Tourmaline

The B isotope composition of tourmaline (n = 117) ranges from −21.6 to 9‰ (Fig. 13a). The $\delta^{11}B$ values for Proterozoic deposits range from −16 to −9‰ (Figs. 13a, b). Archean deposits hosted in the Dharwar Craton have $\delta^{11}B$ values that spread mainly between −5 and 9‰, with a bimodal distribution with a main mode about −2.5‰ and a second mode about 4‰. The $\delta^{11}B$ values for the Archean Yilgarn Craton are the lowest and range between −24 and −18‰. These data are similar to $\delta^{11}B$ values of tourmaline compiled by Trumbull et al. (2020) from orogenic gold deposits worldwide, ranging between −24.8 and 19.8, with two modes at −15 and −2‰.

3.1.9 Silicon in Silicates

The silicon isotope composition of quartz (n = 19) and sericite (n = 11) range from −0.5 to 0.8‰ and from −0.3 to 0.4‰, respectively (Fig. 14a). The limited data is from two deposits, Hemlo (Superior Craton) of controversial origin (Ding et al. 1996), and Sawaya'erdun (Tianshan Orogen) (Liu et al. 2007), such that the representativeness of the range of $\delta^{30}Si$ values is limited. No difference in composition is identified for $\delta^{30}Si$ values in relation to host mineral and deposit age (Fig. 14b).

4 Isotope Equilibrium and Temperature of Formation

The isotope composition of a mineral depends on intrinsic and extrinsic factors. Intrinsic factors are related to the crystal structure, mass of the atoms forming molecular bounds in minerals, and isotope diffusion coefficients. These intrinsic factors determine partitioning of light and heavy isotopes of an element between two coexisting phases, the isotopic fractionation. The extrinsic factors comprise the temperature of the system, the pressure, particularly for gaseous phases, the bulk isotopic composition of the system and its components, and the isotope exchange reaction rate which, if fast, enables close system isotopic equilibrium to be reached or, if slow, will yield a kinetic open system in isotopic disequilibrium. The extrinsic factors determine the magnitude of the fractionation between isotopic species, temperature being the most important.

In order to make interpretations from the isotopic composition of minerals, it is thus essential to verify the assumptions about the state of equilibrium of the system in order to use theoretical or experimental fractionations to derive the temperature of equilibrium, or the bulk isotopic composition of the system and its components. Verification of equilibrium is best achieved comparing the composition of isotopic phases using δ–δ diagrams (Criss et al. 1987). In δ–δ diagrams, two coexisting phases in a closed system, minerals for example, will plot on the isotherm of the temperature of equilibrium, which is determined by the fractionation between the two species. If mineral pairs formed at the same temperature, but in isotopic systems with different bulk compositions, the data will plot along the same isotherm. If minerals formed at different temperatures in a system with a bulk constant isotopic composition, data will plot in an array orthogonal to isotherms.

δ–δ diagrams are drawn for quartz-silicate/borate/tungstate (Fig. 15), quartz-carbonate (Fig. 16), and sulfide-sulfide

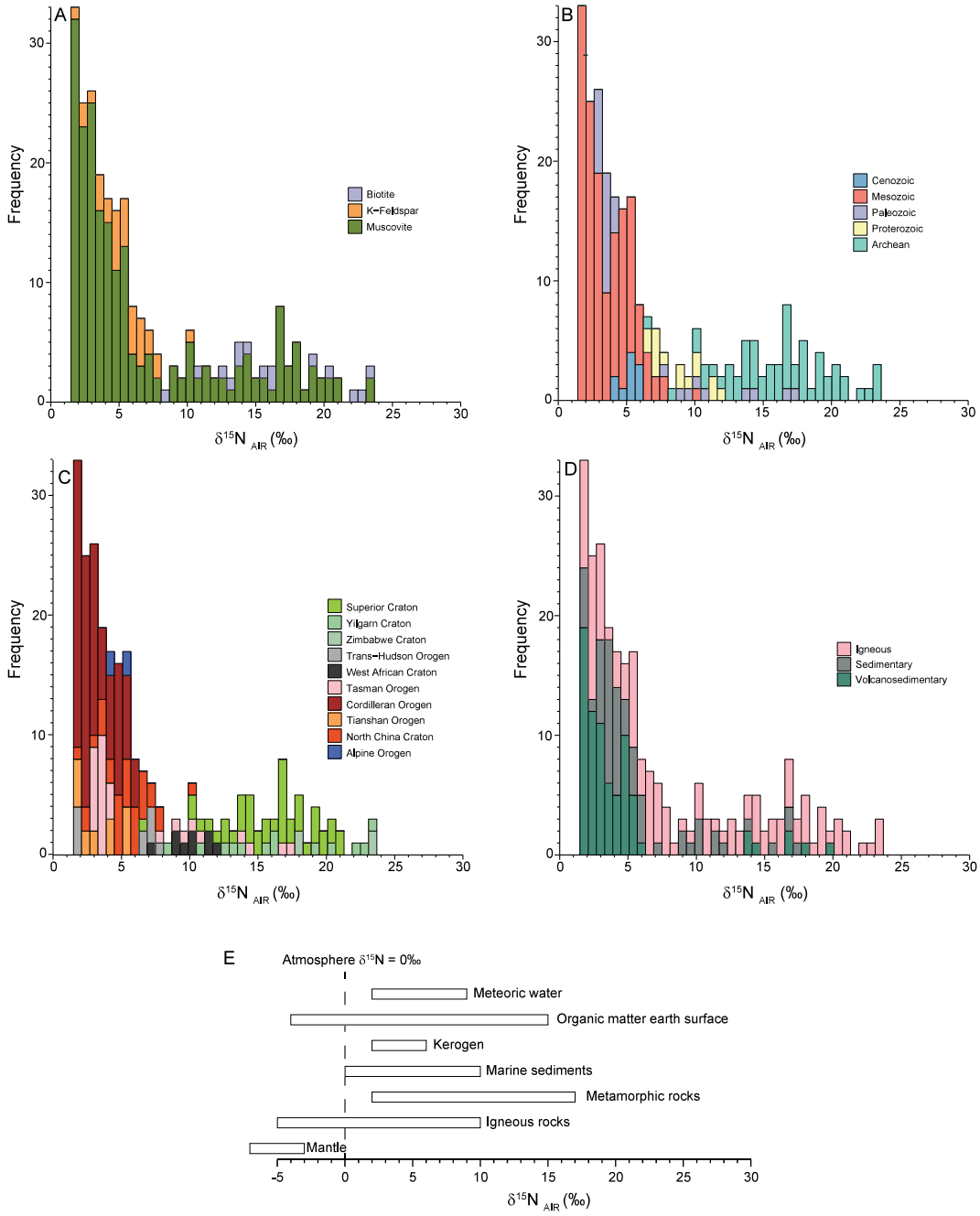

Fig. 12 Histograms showing $\delta^{15}N$ values of minerals from veins from orogenic gold deposits based on: **a** mineral; **b** age of deposit; **c** craton or orogen hosting deposit; and **d** country rock of deposits. **e** $\delta^{15}N$ values of various geological reservoirs are (Peters et al. 1978; Haendel et al. 1986; Minagawa and Wada 1986; Bebout and Fogel 1992; Compton et al. 1992; Williams et al. 1995; Wu et al. 1997; Ader et al. 1998; Jia and Kerrich 2000; Sephton et al. 2002; Gu 2009)

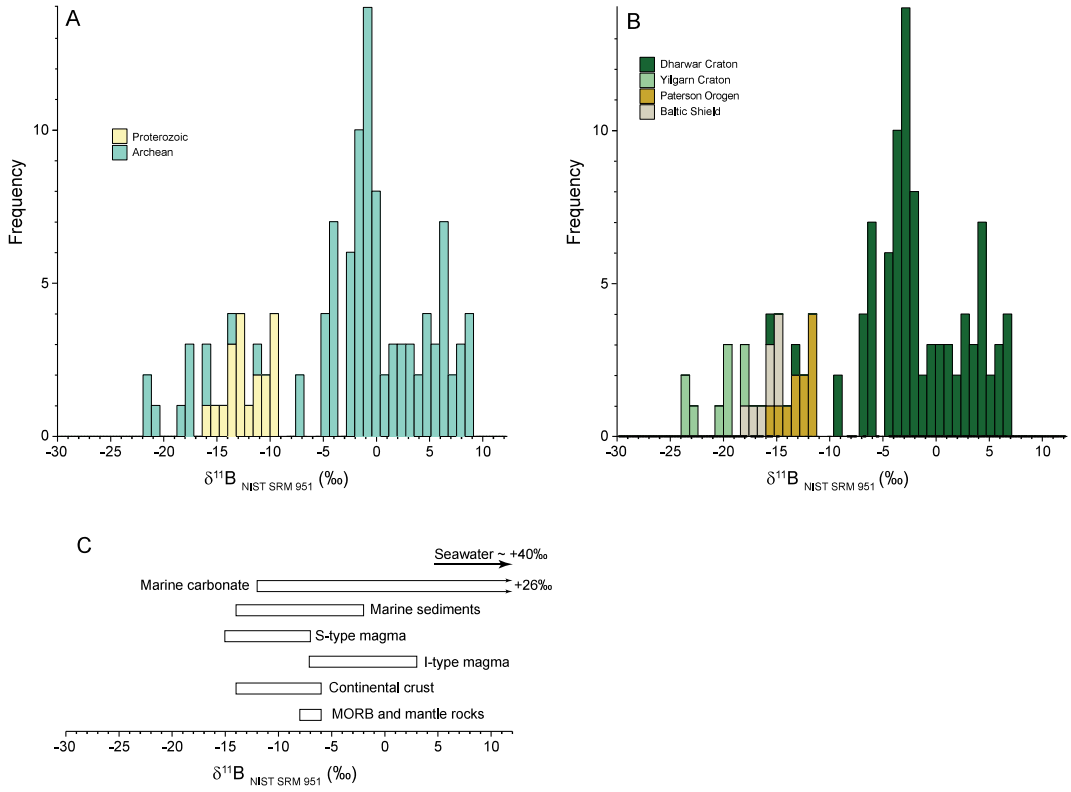

Fig. 13 Histograms showing $\delta^{11}B$ values of tourmaline from veins from orogenic gold deposits based on: **a** the age of the deposit; and **b** the craton or orogen hosting deposits. **c** $\delta^{11}B$ values of various geological reservoirs (Palmer and Swihart 1996; van Hinsberg et al. 2011; Lambert-Smith et al. 2016; Marschall et al. 2017; Trumbull and Slack 2018)

(Fig. 17). Quartz-muscovite mineral pairs from the same sample form a linear array that is parallel to isotherms (Fig. 15a). The data array is centered on the 350 °C isotherm calculated using Vho et al. (2019), which indicates that most quartz-muscovite pairs are approaching isotopic equilibrium near 350 °C. Few mineral pairs plot outside the array, which indicate either isotopic equilibrium at higher/lower temperatures, or isotopic disequilibrium. Using the fractionation of Vho et al. (2019), 60 of the 68 samples plot between the 250 and 550 °C isotherms. An apparent lower temperature of equilibrium is documented for Mesozoic age deposits (Fig. 15a), but this trend is related to the fact that five of the seven quartz-muscovite with temperatures below 350 °C are from the Alleghany district, Cordilleran Orogen (Böhlke and Kistler 1986). Quartz-sericite pairs show a similar distribution (Fig. 15b), but data are mostly centered along the 450 °C quartz-muscovite isotherm. Quartz-biotite pairs (Fig. 15c) show more scatter than quartz-muscovite, but are mostly centered on the 350 °C isotherm. Quartz-chlorite pairs (Fig. 15d) show a similar distribution than that of quartz-biotite pairs, although a number of samples yield large $\Delta_{qz\text{-}chl}$, up to 12‰, which clearly indicates these mineral pairs were not in isotopic equilibrium. Quartz-albite (Fig. 15e) pairs plot mainly parallel to 250 °C isotherm. Quartz-tourmaline pairs (Fig. 15f) form an array centered on the 450 °C isotherm using Vho et al. (2019), but would be around the 350 °C isotherm using the fractionation of Kotzer et al. (1993), which has

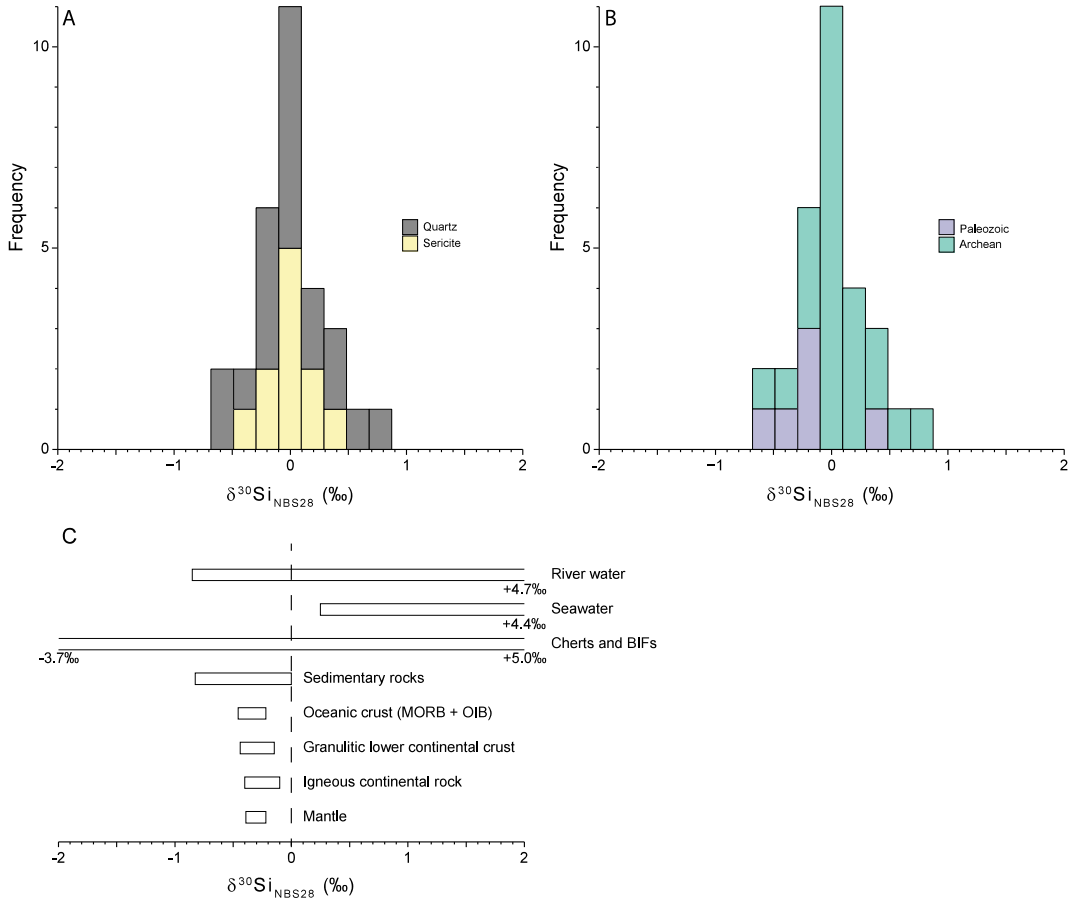

Fig. 14 Histograms showing $\delta^{30}Si$ values of minerals from vein from orogenic gold deposits based on: **a** mineral; and **b** age of deposit. **c** $\delta^{30}Si$ values of various geological reservoirs (Poitrasson 2017 and reference therein)

been defined using Proterozoic and Archean orogenic gold-bearing veins. Several samples have small (~1‰) or large (< 7‰) $\Delta_{qz\text{-}tur}$ values that indicate that these samples are not in isotope equilibrium. Finally, quartz-scheelite pairs scatter in the δ–δ diagram (Fig. 15 g), with several pairs with small (~3‰) or large (< 12‰) $\Delta_{qz\text{-}sch}$ values that indicate that these samples are not in isotope equilibrium. For all quartz-silicate/borate/tungstate pairs, there is no obvious trends with the composition of the country rocks, or age of the deposit.

Quartz-ankerite mineral pairs form a broad array parallel to isotherms (Fig. 16a), but with a large proportion of samples with fractionations too small or too large to record isotopic equilibrium at geologically reasonable temperatures (250–550 °C; (Goldfarb et al. 2005). Both quartz-calcite (Fig. 16b) and quartz-dolomite (Fig. 16c) also form broad arrays along isotherms, but data distribution also shows a trend of high $\delta^{18}O$ values for calcite and dolomite (< 25‰), that indicates isotope disequilibrium with coexisting quartz in these samples.

Because the magnitude of $\Delta^{34}S$ between sulfide minerals at equilibrium temperatures between 250 and 550 °C is small (e.g., 1.6 to 0.7‰ for pyrite-chalcopyrite), small $\Delta^{34}S$ variations yield large variations of the calculated temperature of equilibrium, such that temperature estimation using sulfur isotopes is less accurate. Pyrite-chalcopyrite (Fig. 17a) pyrite-sphalerite

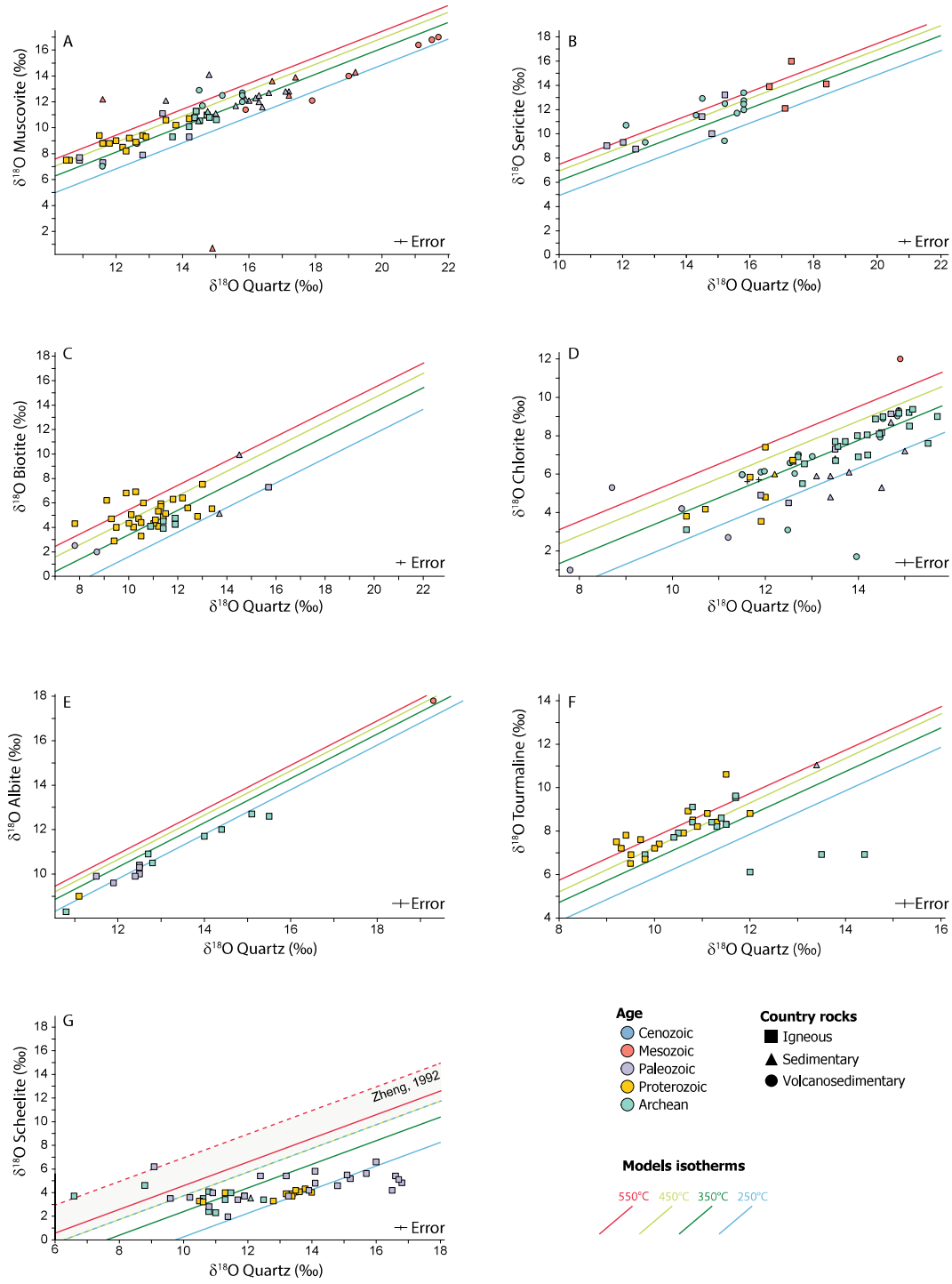

Fig. 15 $\delta^{18}O_{silicates}$ versus $\delta^{18}O_{quartz}$ of coexisting vein minerals with symbols indicating the age and the type of country rocks. Isotherms drawn using oxygen isotope fractionation equations from Vho et al. (2019) for **a**, **b**, **c**, **d**, **e**, **g** and **h** and from Clayton et al. (1972) and Wesolowski and Ohmoto (1986) for **f**

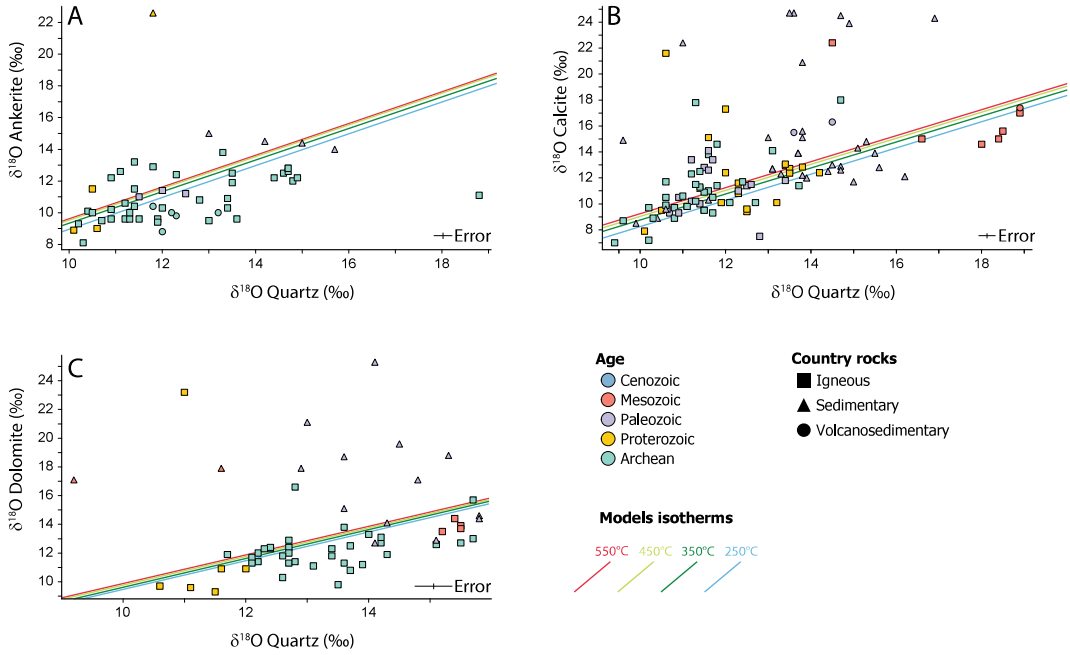

Fig. 16 $\delta^{18}O_{carbonate}$ versus $\delta^{18}O_{quartz}$ of coexisting vein minerals with symbols indicating the age and the type of country rocks. Isotherms drawn using O isotope fractionation equations from Vho et al. (2019) for **a**, and **c**, and from Clayton et al. (1972) and Wesolowski and Ohmoto (1986) for **b**

(Fig. 17b) and pyrite-galena (Fig. 17c) pairs similarly plot as broad arrays parallel to isotherms. For these mineral pairs, only a small proportion of samples show small or large fractionations that indicate sulfur isotope disequilibrium. Most data plot close to the 350 °C isotherm indicating isotope equilibrium. A few pyrite-pyrrhotite pairs scatter in the δ-δ diagram (Fig. 17d), indicating sulfur isotope disequilibrium. Sphalerite-chalcopyrite (Fig. 17e) and sphalerite-galena (Fig. 17f) pairs, similar to most pyrite-sulfide pairs, plot in broad arrays centered along the 350 °C isotherm. Finally, the galena-chalcopyrite δ–δ diagram (Fig. 17 g) shows a broad array parallel to isotherms, but at low calculated temperatures (circa 150 °C).

In summary, quartz-silicate, quartz-carbonate, and sulfide-sulfide mineral-pairs that display evidence for isotopic equilibrium between the 250–550 °C yield an average temperature of 360 ± 76 °C (σ = 1, n = 332) without evidence for secular change with the age of formation of then orogenic gold deposits.

5 Discussion

5.1 Secular Variations in Mineral and Fluid Inclusion Compositions

Figure 2a shows that $\delta^{18}O$ values of quartz from Archean (8–16‰) and Proterozoic (8–16‰) age deposits broadly overlap with Paleozoic (9–17.5‰), Mesozoic (10–22.5‰) and Cenozoic (10–17.5‰) age deposits, yet Phanerozoic age deposits yield slightly higher $\delta^{18}O$ values (9–22.5‰) than Precambrian age deposits (8–16‰). Figure 6b, likewise shows that carbonate minerals from Archean and Proterozoic age deposits typically have lower $\delta^{18}O$ values (7–15‰) than that of Paleozoic (9–25‰) and Mesozoic (8–20‰) age deposits. The change in quartz and carbonate oxygen isotope composition with age of deposit (Figs. 2a and 6b), is not continuous with a reversal to lower $\delta^{18}O$ values for Cenozoic age deposits, casting doubt on a secular evolution

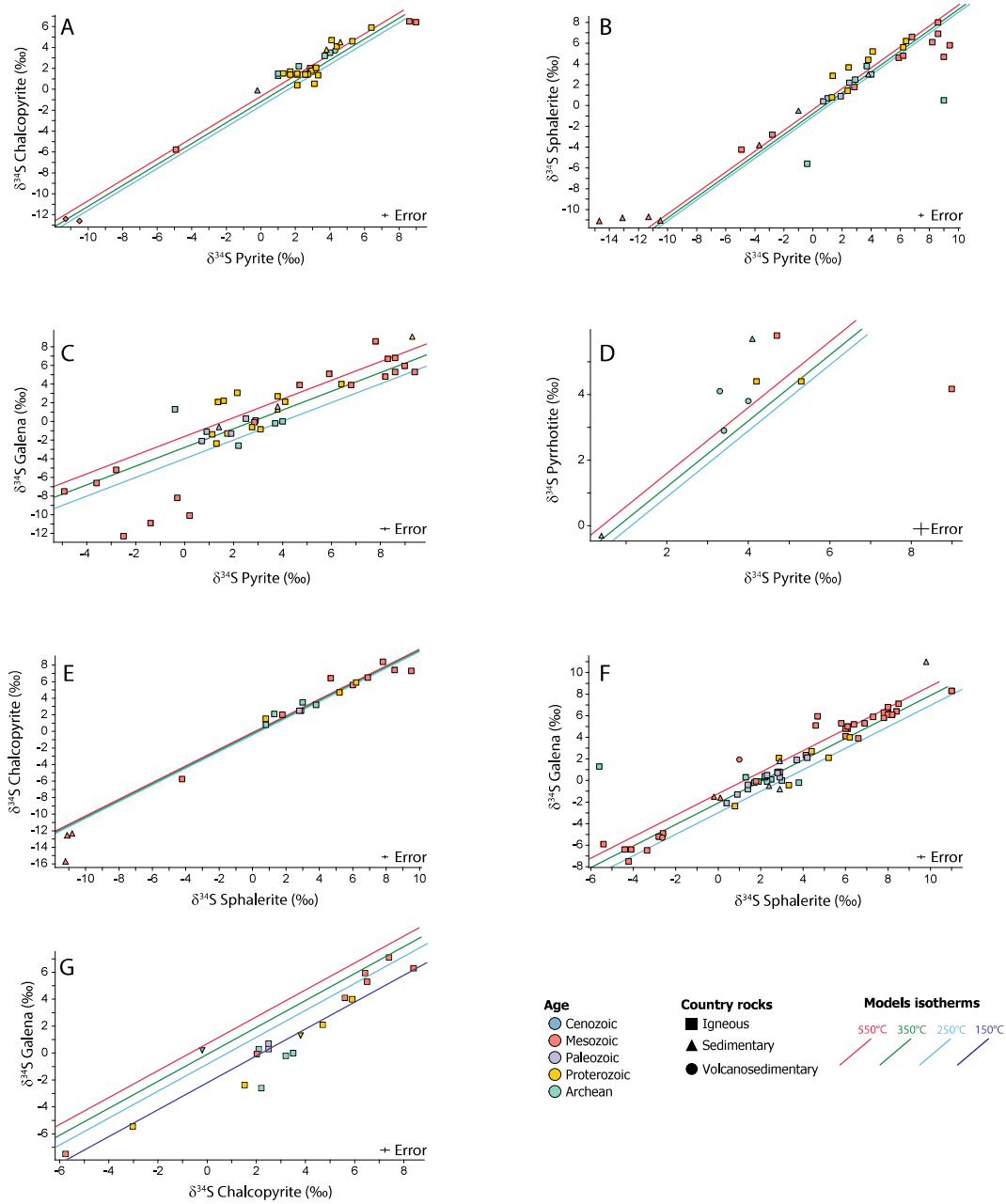

Fig. 17 $\delta^{34}S_{Sulfide}$ versus $\delta^{34}S_{Sulfide}$ of coexisting vein sulphide minerals with symbols indicating the age and the type of country rocks. Isotherms drawn using S isotope fractionation equations from Kajiwara and Krouse (1971) for a, b, d and f, from Li and Liu (2006) for c and e, and from Liu et al. (2015) for g

of the composition of hydrothermal fluids in orogenic gold deposits, as suggested by Goldfarb and Groves (2015). As shown in Fig. 2c, the lower Archean quartz $\delta^{18}O$ values are dominantly for orogenic gold deposits hosted by igneous rocks, whereas Phanerozoic age deposit

higher $\delta^{18}O$ values are characteristic for deposits hosted by sedimentary and volcano-sedimentary country rocks. Figure 6d shows a similar pattern where carbonate with lower and higher $\delta^{18}O$ values correspond to Archean and Proterozoic age deposits dominantly hosted, respectively, by igneous or sedimentary and volcano-sedimentary country rocks.

Less abundant data for other silicate minerals do not allow analysis by age of deposit. In contrast, carbonate mineral $\delta^{13}C$ values do not display a distribution by age of deposit, with the exception of the low $\delta^{13}C$ values from deposits of the Appalachian Orogen, which indicates this a provincial feature (Fig. 9b). Similarly, silicate (Fig. 7b) and inclusion fluid[3] (Fig. 8b) δD values do not display different distributions based on the age of the deposits, with the exception of the low values from the Mesozoic Cordillera Orogen deposits. Sulfide sulfur in deposits hosted by igneous and volcano-sedimentary rocks does not display compositional variations related to the deposit age (Fig. 11). In contrast, deposits hosted in sedimentary rocks show different but overlapping ranges of $\delta^{34}S$ values with age. Chang et al. (2008) showed that Phanerozoic orogenic gold deposits hosted in sedimentary rocks have sulfide $\delta^{34}S$ values that closely track that of seawater sulfate at the age of the host rocks. This result was interpreted to record leaching of reduced seawater sulfate from the sedimentary country rocks. Likewise, Goldfarb et al. (1997) showed that the Juneau district Cenozoic orogenic gold deposits have $\delta^{34}S$ values that follow those of their Phanerozoic sedimentary host rocks. Thus, the sulfur isotope composition of orogenic gold deposits hosted in sedimentary rocks vary with the age of the host rocks following the secular variation of seawater sulfate, but with no evidence of secular variation related to the age of the deposits.

The less abundant data for N (Fig. 12b), B (Fig. 13a) and silicon (Fig. 14b) allows for less definitive assessments of secular variations in composition. The N isotope composition is characteristically higher for Archean (11–24‰) and Proterozoic (7–12.5‰) compared to Paleozoic- (2.5–14‰) and Mesozoic- to Cenozoic-aged deposits (5–7‰: Fig. 12b). The decrease in $\delta^{15}N$ values with decreasing deposit age has been ascribed to progressive mantle degassing ($\delta^{15}N = -5‰ + /-2‰$) into the atmosphere ($\delta^{15}N = 0‰$), and the gradual sequestration of heavier atmospheric N_2 into sedimentary rock micas (Jia and Kerrich 2004; Kerrich et al. 2006). However, other studies suggest that atmospheric $\delta^{15}N$ values were constant through time and that isotopic variations in sedimentary rocks reflect isotopic fractionation related to fluid-rock interaction and/or biogenic activity (Cartigny and Marty 2013).

The compilation shows that Archean age deposits have mostly higher $\delta^{11}B$ values than Proterozic age deposits (Fig. 13a). However, recent studies show that several Archean deposits also have low tourmaline $\delta^{11}B$ values, such as in Val-d'Or (Beaudoin et al. 2013; Daver et al. 2020) and the Hattu schist belt (Molnár et al. 2016). Finally, the limited amount of silicon isotope compositions does not display a trend with age (Fig. 14b).

5.2 Temperature Variations

5.2.1 Isotopic Disequilibrium

Most minerals pairs plot between the 250–550 °C isotherms, temperatures typical for the formation of orogenic gold deposits, thus suggesting widespread isotopic equilibrium for quartz-silicates/borate/tungstate and sulfide-sulfide pairs. In contrast, quartz-carbonate pair $\delta^{18}O$ values are scattered with only few pairs along 250–550 °C isotherms suggesting common isotopic disequilibrium.

Diachronous formation of quartz and carbonate could explain such disequilibrium, although quartz and carbonate are commonly paragenetically coeval in orogenic gold deposits. Isotopic exchange can also occur between mineral-pairs during cooling by volume diffusion (Giletti 1986). As shown by Sharp and Kirschner (1994), the degree of retrograde oxygen diffusion

[3] Factors controlling fluid inclusion isotopic data are complex and described in more detail below.

between quartz and calcite depends of the closure temperature of quartz which, in turn, depends of its grain size, oxygen diffusion coefficient and cooling rate. They showed that for quartz grains in a large reservoir of calcite, resetting below 400 °C will only occur for small quartz grain sizes. Consequently, retrograde diffusion exchange between quartz and calcite in veins is unlikely to explain scattered data in δ_{Qtz}–δ_{Carb} space (Fig. 16). Late infiltration of low temperature fluids can significantly alter the $\delta^{18}O$ value of calcite and disturb the initial isotopic equilibrium between co-genetic minerals (Sharp and Kirschner 1994). This low temperature resetting has been proposed to explain the common isotopic disequilibrium documented for carbonates with high $\delta^{18}O$ values compared to quartz (Kontak and Kerrich 1997; Beaudoin and Pitre 2005): Fig. 16). Because veins commonly experienced successive deformation events (as folded or sheared veins), such late fluid circulation can easily be channelized in newly formed fractures.

5.2.2 Secular Variations in Temperature of Formation of Orogenic Gold Deposits

Goldfarb et al. (2005) suggested that Phanerozoic and Paleoproterozoic orogenic gold deposits formed at lower temperatures (250–350 °C) that older Archean deposits (325–400 °C). However, they acknowledged that each age group of orogenic gold deposits displayed large, and overlapping, ranges of temperature of formation. For mineral pairs showing isotope equilibrium, there is no secular trend of changing equilibrium temperature with age of deposit (Figs. 15, 16 and 17). This observation is independent of the fractionation used to compute the temperature, as the different fractionations will only shift the nominal value of the temperature, not the data distribution along isotherms. Thus, the stable isotope composition of vein minerals does not support the interpretation of a lower temperature of formation for Proterozoic and Phanerozoic orogenic gold deposits, compared to higher temperature Archean age orogenic gold deposits.

5.3 Composition of Hydrothermal Fluids and Dissolved Elements

In the following sections, the $\delta^{18}O$ and δD values of H_2O and $\delta^{13}C$ values of CO_2 are calculated from minerals isotopic composition at temperatures of 250–550 °C for mineral pairs that show evidence of isotope equilibrium. $\delta^{34}S$ values of H_2S have not been calculated because isotope fractionation between sulfides and H_2S are small (< 1‰) between 250 and 550 °C (Li and Liu 2006). The source of H_2S is discussed based on $\delta^{34}S$ values of sulfides.

5.3.1 Water

Metamorphic versus magmatic water. The two most common sources of fluids proposed for orogenic gold deposits are magmatic and metamorphic water. As reviewed by Goldfarb and Groves (2015), the inconsistent timing between magmatism and orogenic gold deposit formation, and lack of a specific magmatic association, both argue against the ubiquity of magmatic fluids in the formation of orogenic gold deposits.

Most of the calculated water compositions plot in the field for metamorphic water, but a small proportion of analyses also plot in the field for magmatic water and a few plot outside both fields (Figs. 18a, b; Sheppard 1986). Magmatic water has been argued in some cases (Li et al. 2012; Zeng et al. 2014; Deng et al. 2015), but this interpretation is based on fluid $\delta^{18}O$ and δD values between −0.2 and 6‰ and −96 and −52‰, respectively, that plot largely outside of the magmatic water field, and are too low for the inferred granitic magma source. Thus, metamorphic water is the more common fluid source, and in most cases the only likely fluid source for the formation of orogenic gold deposits. The variation of oxygen and hydrogen isotopes composition of metamorphic water(s) documented on Fig. 18 probably reflect that fluids were sourced from metamorphism of variable proportions of sedimentary and igneous rocks in the crust.

Evidence of meteoric water in fluid inclusions. Fluid inclusions are trapped either during crystal

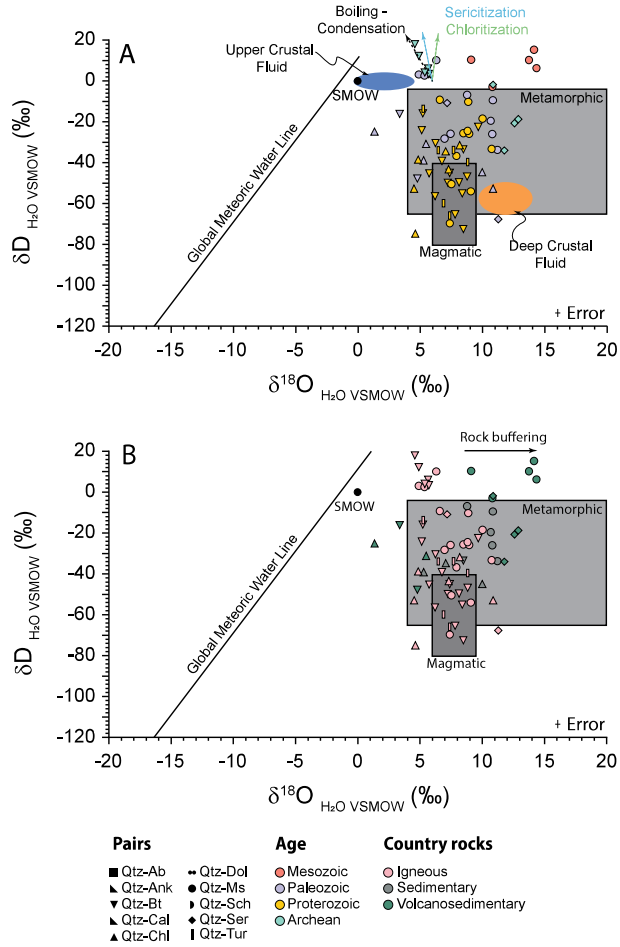

Fig. 18 Diagrams showing the variation of $\delta^{18}O$ and δD values of H_2O calculated from quartz and OH-bearing minerals. **a** δD_{H2O} versus $\delta^{18}O_{H2O}$ with symbols indicating the age of deposits, and **b** the type of country rocks. The high δD values are interpreted to reflect the effect of evaporation–condensation cycles, whereas higher $\delta^{18}O$ reflect O isotope buffering by fluid-rock interactions. The Global Meteoric Water Line is derived from Craig (1961), whereas the metamorphic and magmatic water boxes are from Sheppard (1986)

growth (primary) or in cracks during late fluid circulation (secondary). Caution must be exercised using isotope composition of fluid inclusions because the mechanical or thermal decrepitation leach methods extract all populations of fluid inclusions, some of which not associated with gold formation. It has been shown by Faure (2003) than thermal decrepitation yield inaccurate δD values, possibly because of uncontrolled reactions between released H_2O and Si–OH bounds in quartz, for example. Likewise, Gaboury (2013) showed that fluid inclusions have different hydrocarbon compositions as a function of the temperature of decrepitation. As an example, Foley et al. (1989) showed bulk extract contained two types of fluid inclusions with distinct δD values at Creede (Colorado, USA). This is particularly likely in orogenic gold deposits where veins are commonly deformed and thus may have trapped various fluids during and/or after mineralization. For example, in laminated veins, most fluid inclusions are secondary (Ridley and Diamond 2000). Pickthorn et al. (1987) reviewed evidence for discrepancy between fluid inclusion and mica δD values and concluded to mixing of various generations of fluid inclusions, including late meteoric water trapped in secondary inclusions in the host minerals. This was contested by Nesbitt et al. (1987) on the basis that various mixtures of fluid inclusions should yield a mixing line between two end members, contrary to the low variance of δD values.

As shown on Fig. 19, micas are commonly out of isotopic equilibrium with fluid inclusions trapped in quartz from the same vein. Isotopic

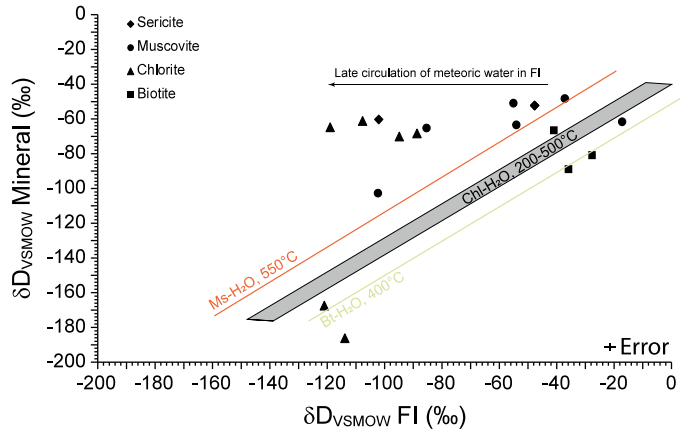

Fig. 19 $\delta D_{Mineral}$ versus δD_{FI} coexisting OH-bearing mineral and fluid inclusions from a same sample. Isotherms have been drawn using mineral-H_2O H isotope fractionations of Suzuoki and Epstein (1976) for muscovite and biotite and from Graham et al. (1987) for chlorite. The grey area represents the uncertainty associated to the chlorite-H_2O H isotope fractionation of Graham et al. (1987) between −40‰ and −30‰ between 200 and 500 °C

disequilibrium is well documented for chlorite and some sericite/muscovite displaying high δD values (∼-60‰) compared to the δD values of coexisting fluid inclusion (<-60‰). Such disequilibrium has been interpreted to record infiltration of late, low δD meteoric water or a mixture of several types of fluid inclusions with different hydrogen isotope compositions (Goldfarb et al. 1991). Fluid inclusions (Figs. 8a) and OH-bearing minerals (Fig. 7b) low δD values are mainly documented from Mesozoic and Cenozoic deposits, and are commonly interpreted to result from late meteoric water infiltration disconnected with the formation of the deposits (Nesbitt et al. 1989; Zhang et al. 1989; Madu et al. 1990; Goldfarb et al. 1991; Shaw et al. 1991; Rushton et al. 1993; Apodaca 1994; Jia et al. 2003). However, similar low δD values are also documented for older deposits. In deposits from Trans-Hudson terrane (Figs. 8a, b), Liu (1992) considered that meteoric water circulated in the vein structure, but after the formation of the deposit. In contrast, Billstrom et al. (2009) suggest that low δD values in Baltic Shield Paleoproterozoic age deposits could reflect infiltration of surface water during gold deposition.

Fluid Mixing. Figures 20a, b, c and d show the variation of $\delta^{18}O_{H2O}$ and δD_{H2O} values as a function of the temperature of equilibrium between pairs of minerals. For both isotopes, data is spread along a linear trend between low $\delta^{18}O$ (∼2‰), high δD (∼10‰) values at low temperatures (∼250 °C), and high $\delta^{18}O$ (∼12‰), low δD (∼-100‰) values at high temperatures (∼550 °C) of equilibrium. This trend is similar to that documented by Beaudoin and Chiaradia (2016) for quartz and tourmaline from orogenic veins from the Val-d'Or vein field, which was interpreted to result from mixing between a low temperature upper crustal fluid and a high temperature deep-seated crustal fluid. Data for orogenic gold deposits (Figs. 20a,b,c,d) show that the same mixing trend between similar fluid end-members is recorded for deposits of all ages (Archean to Cenozoic), hosted in different country rock types, suggesting that fluid mixing between two common reservoirs may be an important process documented in orogenic gold deposits of all ages, worldwide, yet poorly documented in literature. The high $\delta^{18}O$—low δD—high T deep-seated crustal fluid is likely metamorphic in origin, whereas the low $\delta^{18}O$—high δD—low T upper crustal fluid is water of surficial origin with a long history of water–rock reactions, perhaps not unlike long residence water in cratons, as reviewed by Warr et al.

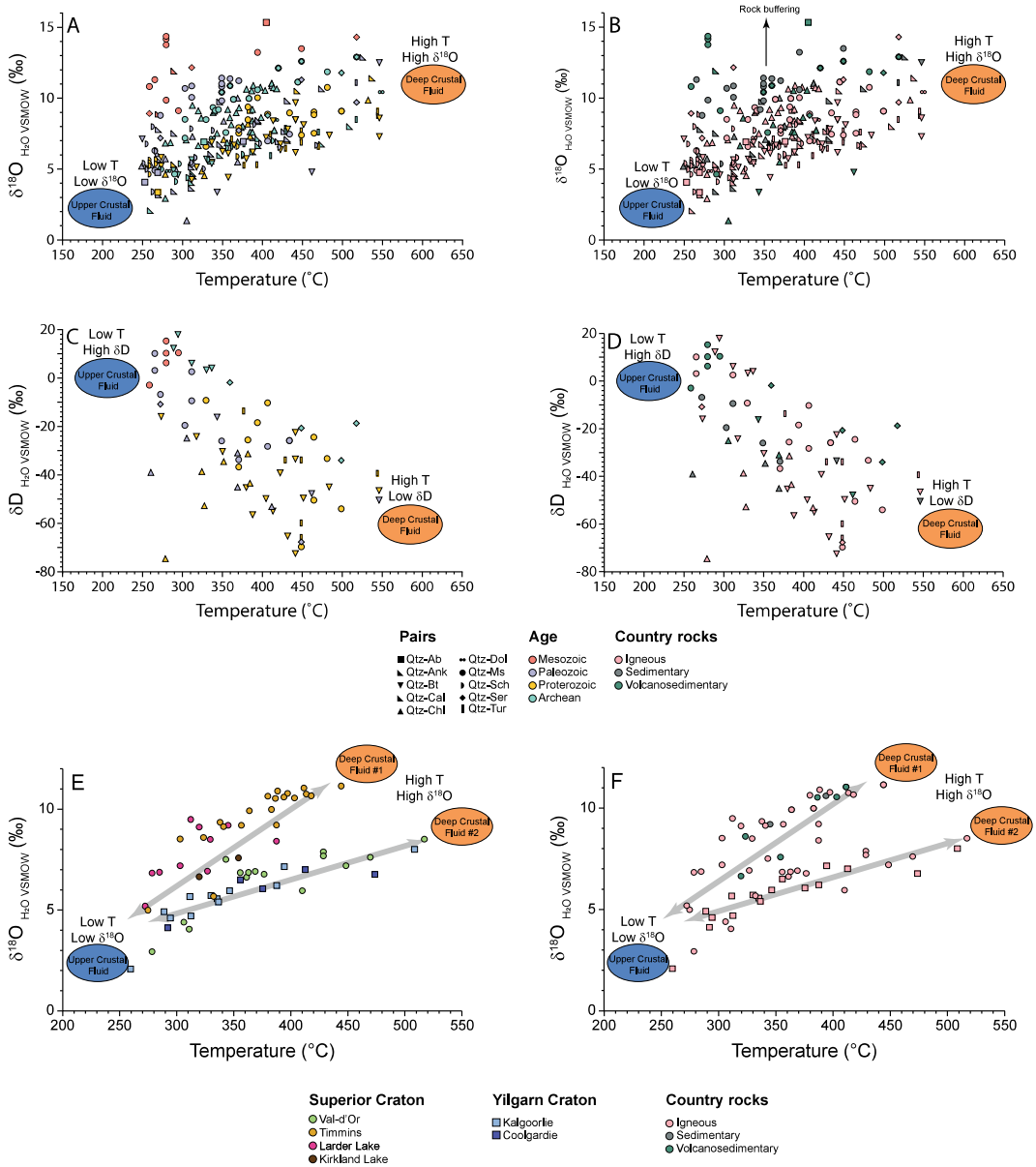

Fig. 20 Diagrams showing the variation of $\delta^{18}O$ of H_2O calculated from quartz and OH-bearing minerals as function of temperature calculated from mineral pairs based on: **a** the age of deposits; and **b** the type of country rocks. Diagrams showing the variation of δD of H_2O calculated from quartz and OH-bearing minerals as function of temperature calculated from mineral pairs based on: **c** the age of deposits and **d** the type of country rocks. The broad linear arrays in **a**, **b**, **c** and **d** suggest mixing between a low temperature, low $\delta^{18}O$, high δD (interpreted as an upper crustal) and a high temperature, high $\delta^{18}O$, low δD (interpreted as a deep crustal) fluids. Diagrams showing the variation of $\delta^{18}O$ of H_2O calculated from quartz and OH-bearing minerals as function of temperature calculated from mineral pairs based on: **e** the district; and **f** the type of country rocks. The shift in $\delta^{18}O$ values between different districts could suggest provinciality on the fluid, that is that the deep-seated fluid reservoir varies slightly in composition between orogenic gold vein districts

(2021). The ultimate origin of the surficial water, obscured by water–rock exchange, may be difficult to decipher in several deposits. High δD_{H2O} values, up to 0‰, in the Wiluna deposit (Yilgarn) have been interpreted to result from mixing of surface water, at shallow levels, with metamorphic-magmatic fluids (Hagemann et al. 1994). Boiron et al. (2003) showed that the deep-seated fluid was the dominant reservoir involved in the first step of the vein formation followed by progressive infiltration of surficial water during basement uplift. It is known that crustal rocks porosity contains water deep in the crust (Smithson et al. 2000). This water may have been trapped since rock formation or may have infiltrated from surface (seawater or meteoric) slowly reacting with country rocks along the fluid pathways. If fluid mixing has not been commonly identified in orogenic gold districts, the data compilation indicates that most deposits, in which we can interpret a temperature of equilibrium and a H–O fluid composition from mineral pairs, plot along a broad array that we interpret as a mixing line between two common reservoirs. Beaudoin et al. (2006) showed that the regional change in oxygen isotope composition of orogenic gold deposits of the Val-d'Or vein field can be reproduced by simulating fluid flow and oxygen isotope transport and reaction of the deep-seated fluid in rocks saturated by the upper crustal fluid end-members. Infiltration of the deep-seated fluids along the higher permeability shears and fractures of the orogenic gold deposits resulted in mixing with the upper crustal fluids filling the host rocks porosity, thus yielding the mixing lines shown in Fig. 20. Mixing of various proportions of fluids from different reservoirs also explains the gradual change in composition between deposits in one district, as shown in the Val-d'Or (Beaudoin and Pitre 2005) and Victoria (Gray et al. 1991) vein fields.

Fluid buffering. As shown in Figs. 2c, 6d, the highest quartz and carbonate $\delta^{18}O$ values are documented in deposits hosted dominantly in volcano-sedimentary and sedimentary rocks, consistent with the interpretation that isotopic oxygen exchange between fluids and sedimentary rocks leads to ^{18}O-enriched quartz (Böhlke and Kistler 1986; Goldfarb et al. 1991, 2004; Boer et al. 1995; Zhang et al. 2006) and carbonates (Böhlke and Kistler 1986; Steed and Morris 1997). For carbonates, some values enriched in ^{18}O also likely reflect a late, retrograde, and low-temperature re-equilibration with a surface-derived fluid.

Figures 18b and 20b shows that most $\delta^{18}O_{H2O}$ values higher than those along the mixing trend, are from deposits hosted in sedimentary or volcano-sedimentary rocks. This suggests oxygen isotope buffering of the fluids by sedimentary and volcano-sedimentary country rocks, which is detected in sedimentary rocks because of their heavier oxygen isotopic composition (Sheppard 1986).

Provinciality. Figures 20e and f present $\delta^{18}O_{H2O}$ values as function of temperature for the Archean Yilgarn (Kalgoorlie and Coolgardie districts) and Superior (Val-d'Or, Timmins, Larder Lake, and Kirkland Lake districts) cratons. Data displays two trends between a common low $\delta^{18}O_{H2O}$—high δD—low temperature upper crustal fluid endmember, and two slightly different deep-crustal fluid endmembers distinguished by their oxygen isotope composition. Deep crustal fluid #1 is characteristic of the Kirkland Lake, Larder Lake, and Timmins Superior Craton districts, and has a $\delta^{18}O_{H2O}$ about 4‰ higher than deep crustal fluid #2, which is defined by deposits of Superior Craton Val-d'Or, and Yilgarn Craton Kalgoorlie and Coolgardie, districts. This suggests that the deep-seated fluids were sourced from rocks at depth with a slightly different oxygen isotope composition, likely reflecting different proportions of igneous and sedimentary rocks in the crustal segment undergoing prograde metamorphism, such that the deep-seated fluid reservoir varies slightly in composition between orogenic gold vein districts. The difference in end-member composition cannot be an artifact of water–rock reactions because deposits from both trends are hosted dominantly by igneous rocks (Fig. 20f).

Origin of high δD fluids. The formation of the gold-bearing quartz vein is commonly associated with the precipitation of micas in the veins and host rock, or micas formed by hydration of host-

rock minerals (Groves et al. 1998; Ridley and Diamond 2000; Eilu and Groves 2001; Craw et al. 2009). Muscovite and chlorite are the two main micaceous minerals in orogenic gold deposit. Here, we model the evolution of the H–O isotopic composition of water from which micas precipitate progressively in an open system following Rayleigh distillation to determine if mica precipitation can explain the deuterium enrichment, up to 20‰, of the hydrothermal fluids in orogenic system (Fig. 18e, f). Isotopic exchange between fluid and hostrock is not considered. Equations 1 and 2 are modified from Sharp (2017):

$$\delta_{Liq} = [\delta_{Liq} + 1000]F^{(\alpha_{Chl/Ms-Liq}-1)} - 1000, \quad (1)$$

and

$$\delta_{Chl/Ms} = \alpha_{Chl/Ms-Liq}(\delta_{Liq} + 1000) - 1000, \quad (2)$$

where F is the remaining water fraction, at 350 °C and using 1000ln $\alpha_{chlorite\text{-}H2O}$ = −35‰ (Graham et al. 1987) for H, 1000ln $\alpha_{chlorite\text{-}H2O}$ = −0.7‰ (Wenner and Taylor 1971) for O, 1000ln $\alpha_{muscovite\text{-}H2O}$ = −37.8‰ (Suzuoki and Epstein 1976) for H, and 1000ln $\alpha_{muscovite\text{-}H2O}$ = 1.3‰ (Vho et al. 2019) for oxygen.

The composition of water in equilibrium with chlorite and/or muscovite during progressive crystallization of micas follows a D-enrichment trend toward high δD values (Fig. 21c). A 20‰ enrichment in deuterium is reached after consumption of ~40–45% hydrogen to form chlorite or muscovite. During chlorite precipitation, there is a ~0.4‰ ^{18}O enrichment of the residual fluid, for a δD enrichment of ~20‰, whereas muscovite precipitation causes a decrease of fluid $\delta^{18}O$ values of about −0.7‰ for the same deuterium enrichment. In a δD–$\delta^{18}O$ space, muscovitization yields a trend with a steep negative slope whereas chlorite precipitation yields a steep positive slope. The change in δD of fluids during muscovite precipitation could contribute to explain high δD values of the hydrothermal fluid as shown in Fig. 18a.

Seismic rupture of fault veins occurs after a pre-seismic stage during which fluid pressure increases progressively to reach and overcome the lithostatic pressure (Sibson et al. 1988). Seismic rupture occurs once the increasing shear stress reaches a critical value, which then triggers progressive drainage of the overpressured fluid upward along the fault, and an abrupt fluid pressure decrease. This leads to increased effective stress on the fault plane that seals the fault, during which vein mineral precipitates, which reduces permeability of the fault and yield a new cycle of increasing fluid pressure. This cycle can be repeated numerous times, as attested by the typical crack and seal texture of orogenic veins, in the so-called fault-valve model (Sibson et al. 1988; Robert et al. 1995; Cox 2005). It has been shown that these pressure fluctuations can induce water vapor phase separation (Wilkinson and Johnston 1996; Ridley and Diamond 2000). It is likely that lower density vapor will migrate upward along a high permeability structure, separating from the residual liquid in a vein opening. Upon sealing of the vein, the vapor will condense under increasing pressure. The boiling-condensation cycles can be summarized as follow:

$$F_0 \rightarrow V_1 \rightarrow F_1 \rightarrow V_2 \rightarrow F_2 \rightarrow \ldots V_n \rightarrow F_n, \quad (3)$$

where F_0 is the initial fluid, V_n the composition of vapor separated from F_{n-1}, which then condenses in a new fluid F_n and n the number of boiling-condensation cycles (Fig. 21b).

We model the isotope effects during boiling-condensation open-system Rayleigh isotopic fractionation for vapor formation from a fraction of the liquid and assume complete condensation of vapor. This means that the new fluid F_n will have the same isotopic composition as the vapor V_n using Eqs. 4 and 5, modified after Sharp (2017):

$$\delta_{Liq} = [\delta_{Liq,i} + 1000]F^{(\alpha_{Vap-Liq}-1)} - 1000, \quad (4)$$

and

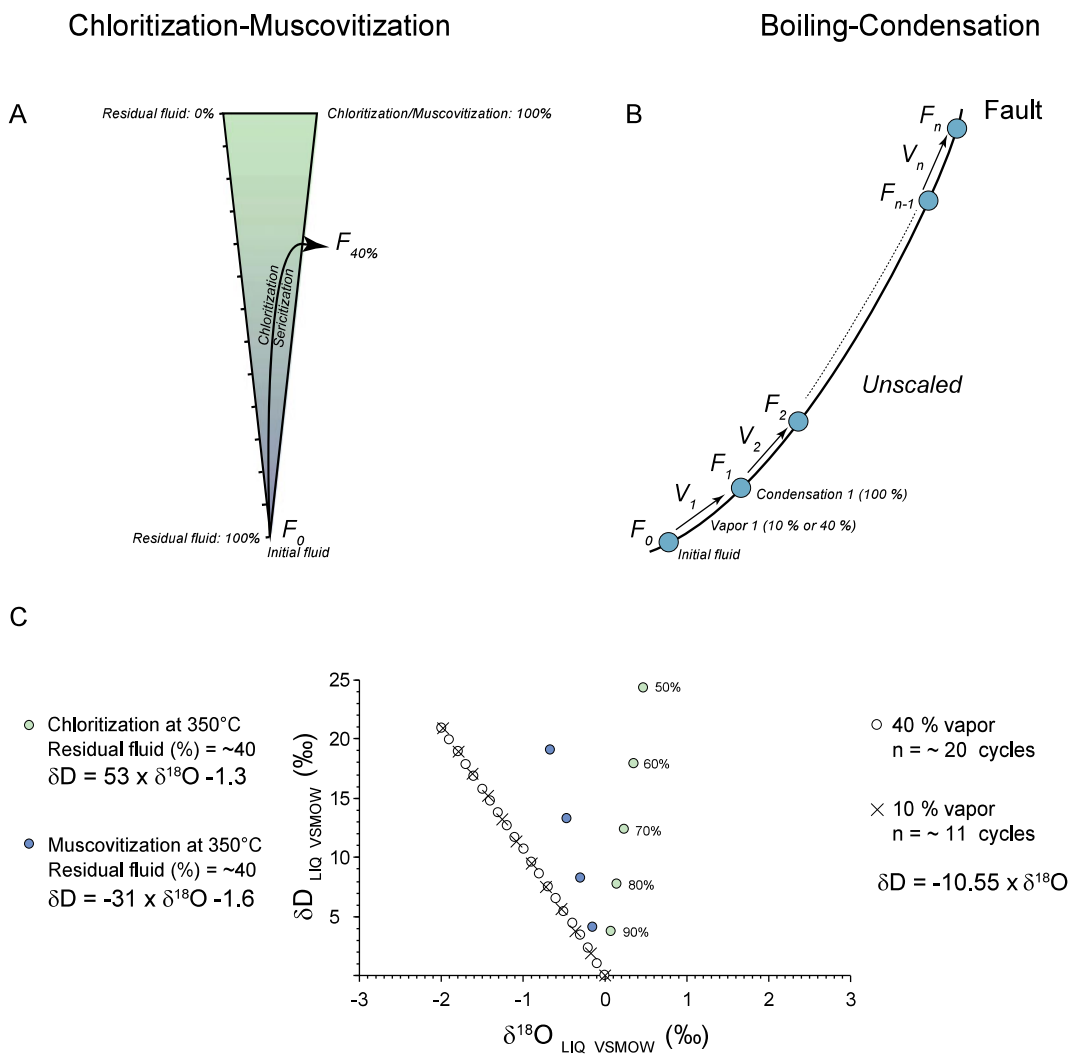

Fig. 21 **a** Conceptual model of the effect of chloritization/sericitization of country rock on the ore fluid. **b** Conceptual model of the successive boiling-condensation cycles related to the fault valve model (Robert et al. 1995). Vapor formation from an over-pressured fluid (F_0) can occur during seismic events. Vapor (V_1) is expected to migrate upward, faster than residual liquid and then to condense entirely (F_1) during re-sealing of fault. This process can be repeated numerous (n) times because of the successive re-opening of the fault during seismic cycles. **c** Quantification of the vector of enrichment in deuterium and depletion in ^{18}O of the evolved fluid (Fn) computed for the different models

$$\delta_{Vap} = \alpha_{Vap-Liq}\left(\delta_{Liq} + 1000\right) - 1000. \quad (5)$$

Using isothermal conditions at 350 °C, considering 10% or 40% of vapor formation from liquid for each successive vapor separation episode, and oxygen and hydrogen isotope fractionation between vapor and liquid from Horita and Wesolowski (1994).

The two scenarios (10 and 40% vapor separation) yield similar linear trends with higher δD and lower $\delta^{18}O$ values for the condensed water, along a vector with a slope of −10.5 (Fig. 21c). The proportion of water evaporation for each cycle (10% or 40%) only changes the magnitude of the isotopic shift (Fig. 21c), and consequently the number of cycles required to reach 20‰

enrichment in deuterium of residual water, and a corresponding depletion of −2‰ in ^{18}O, similar to the maximum fluid δD values in orogenic gold deposits (Figs. 18a, b). Using 10% of evaporation, ∼11 cycles are required to reach the δD value of 20‰, whereas ∼20 cycles are needed with 40% evaporation steps (Fig. 21c). The modeled boiling-condensation trend is consistent with positive δD values (∼20‰) combined with smaller ^{18}O depletion (∼-4‰) of the fluid recorded by equilibration fractionation with hydrogen bearing minerals (Fig. 18a). The boiling-condensation trend is consistent with data with $\delta D_{H2O} > 0‰$ from the Val-d'Or vein field (Beaudoin and Chiaradia 2016) showing similar deuterium enrichment (δD from 0‰ to 29‰) and ^{18}O depletion ($\delta^{18}O$ from 5.9‰ to 2.9‰) of mineralizing fluid.

5.3.2 Source(s) of CO_2

CO_2 plays an important role in the formation of orogenic gold deposits as testified by (i) the common carbonation of country rocks, (ii) the association of gold with quartz-carbonate veins, and (iii) the occurrence of CO_2-rich fluid inclusions trapped in orogenic quartz veins (Smith et al. 1984; Ho et al. 1992). CO_2 has the capacity to buffer the pH of the fluid in a range where the gold complexation with reduced sulfur is increased (Phillips and Evans 2004). Nevertheless, the origin of CO_2 remains debated. Four main carbon reservoirs have been proposed to explain the wide variation of $\delta^{13}C$ values of CO_2; (i) reduced organic carbon in sedimentary rocks (such as graphite, organic matter) with low $\delta^{13}C$ values −26‰, Kerrich (1989); (ii) deep-seated mantle-derived carbon with $\delta^{13}C$ ranging from −10.8 to −1.6‰ (Trull et al. 1993), (iii) magmatic CO_2 ($\delta^{13}C$ from −5 to −2‰; (Taylor 1986), and (iv) seawater-derived carbonate with a $\delta^{13}C$ value near 0‰.

Figure 10 shows the distribution of $\delta^{13}C$ values CO_2 either from fluid inclusion trapped in quartz and scheelite or calculated from quartz-carbonate pairs with equilibrium temperatures in the range 250–550 °C. The $\delta^{13}C$ values of CO_2 display a similar range of values, between −25 and 6‰, as well as a similar distribution, mainly between −12 and 0‰ (Fig. 10a). No trend between $\delta^{13}C$ values and the age of deposit is documented, although all Archean age deposits have $\delta^{13}C_{CO2}$ values above −6‰.

The positive $\delta^{13}C$ values are commonly interpreted as metamorphic CO_2 released during decarbonation reaction of a source with $\delta^{13}C$ near 0‰, such as sedimentary carbonate rocks (Oberthuer et al. 1996; Chen et al. 2008; Scheffer et al. 2017). The low $\delta^{13}C_{CO2}$ values (< −8‰) are mainly documented from deposits hosted in sedimentary rocks (Fig. 10c). This is particularly well illustrated by the Meguma district from the Appalachian/Caledonian Orogen (Fig. 9c), where carbonate minerals have negative $\delta^{13}C$ values ($-25.9‰ < \delta^{13}C < -18.2‰$), which was interpreted by Kontak and Kerrich (1997) to represent the formation of ^{13}C-depleted CO_2 by oxidation of graphite from the sedimentary country rocks (Fig. 9d). Most authors have argued that CO_2 with negative $\delta^{13}C_{CO2}$ values could formed by oxidation/hydrolysis of reduced carbon in sedimentary rocks during metamorphism (Oberthuer et al. 1996; Kontak and Kerrich 1997; Klein et al. 2008; Billstrom et al. 2009).

Nevertheless, some low $\delta^{13}C_{CO2}$ values are also documented from deposits hosted by igneous rocks. One value at −24.1‰ is from fluid inclusions in quartz from the Proterozoic Chega Tudo gold deposit (Brazil), where Klein et al. (2008) argued that the low $\delta^{13}C_{CO2}$ values reflect organic carbon from the carbonaceous schist hosting the porphyritic rocks. The two others values (−25.0‰ and −18.8‰) have been measured from fluid inclusions in scheelite from the Proterozoic intrusive-hosted Björkdal gold deposit, Sweden, (Billstrom et al. 2009), where they argued that these values indicate organic carbon derived from the greywacke-dominated sedimentary rocks that host the intrusion.

The most debated $\delta^{13}C_{CO2}$ values are those between −12 and −1‰ (Fig. 10). Several authors argued that these signatures indicate a deep-seated carbon source, such as sub-continental mantle or an igneous carbon source (Rye and Rye 1974; Shelton et al. 1988; Zhang et al. 1989; Santosh et al. 1995; Oberthuer et al. 1996;

Haeberlin 2002; So et al. 2002; Pandalai et al. 2003; Klein et al. 2007; Billstrom et al. 2009; Sun et al. 2009). Klein et al. (2007) concluded that the wide range of $\delta^{13}C_{CO2}$ values (−10.7 to −3.9‰) do not allow to discriminate a particular source and could reflect leaching of carbon of the country rocks along the fluid pathway. Alternatively, some authors argued that these signatures could also be derived from prograde metamorphism of reduced carbon-bearing sediments in the middle crust (Zhang et al. 1989; Madu et al. 1990; Oberthuer et al. 1996).

5.3.3 Source of H_2S

The sulfide minerals in orogenic gold deposits (Fig. 11) have $\delta^{34}S$ mostly from ~0‰ to 10‰ with a significant number of data tailing to values as low as −30‰. Mantle H_2S has a narrow range of compositions with $\delta^{34}S$ between ~−1.5‰ and ~1.0‰ (Labidi et al. 2013) whereas magmatic H_2S has $\delta^{34}S$ values typically ranging between ~−3.7‰ and ~16‰ (Seal 2006). Ancient marine evaporites record the marine sulfate reservoir with positive $\delta^{34}S$ values mainly between ~10 and ~35‰ (Claypool et al. 1980; Seal 2006). Finally, sedimentary pyrite defines a large range of $\delta^{34}S$ with low values, as low as −50‰, and positive values up to ~16‰. This large range of values reflects variable sulfur isotope fractionation during bacterial and thermochemical sulfate reduction (BSR and TSR). Sulfur isotope fractionation during TSR yields sulfides with 11–43‰ lower than sulfate $\delta^{34}S$ values at 500 °C and 100 °C respectively (Eldridge et al. 2016). During BSR, depletion of ^{34}S is up to 72‰ depending of environmental conditions (Machel et al. 1995; Wortmann et al. 2001; Johnston et al. 2007). In orogenic gold deposits, the range in H_2S sulfur isotope composition can result from mixing of different sulfur reservoirs or sulfur leaching during fluid/rock exchange along the fluid pathway, and changes in physico-chemical conditions (pressure, temperature, fO_2, pH) of the fluid (Schwarcz and Rees 1985; Fedorowich et al. 1991; Thode et al. 1991; Couture and Pilote 1993; Neumayr et al. 2008). Commonly, low $\delta^{34}S$ values (< 10‰) are attributed to BSR sources of reduced H_2S such as from sedimentary rocks (Nie and Bjorlykke 1994; Oberthuer et al. 1996; Nie 1998; Bierlein et al. 2004; Goldfarb et al. 2004; Chen et al. 2008), whereas higher $\delta^{34}S$ values (> 10‰) are attributed to TSR sources of H_2S (Kontak and Smith 1989; Tornos et al. 1997) or igneous sulfur (Hattori and Cameron 1986).

Investigation of mass independent fractionation of sulfur (MIF-S; $\Delta^{33}S$) in hydrothermal systems has been used as a complementary tracer of the source of H_2S. Whereas $\delta^{34}S$ values are sensitive to physico-chemical processes which can modify its isotopic composition along the fluid pathway or at the deposition site, MIF-S is a chemically conservative tracer. By combining $\delta^{34}S$ and $\Delta^{33}S$, several studies of Archean orogenic gold deposits from Yilgarn, Barberton and Abitibi have shown that H_2S is partly derived from Archean sedimentary rocks (Helt et al. 2014; Agangi et al. 2016; Selvaraja et al. 2017; LaFlamme et al. 2018; Petrella et al. 2020). The low variance of $\Delta^{33}S$ values in a deposit has been interpreted to indicate a homogeneous sedimentary H_2S reservoir, such that $\delta^{34}S$ variations in a deposit record variations of the oxidation state of the hydrothermal fluid (LaFlamme et al. 2018; Petrella et al. 2020) or redox reactions with country rocks, as suggested in Neumayr et al. (2008) for the St. Yves gold camp (Yilgarn). On the other hand, $\delta^{34}S$ variations at the deposit or district scales can record the incorporation of H_2S from the local country rocks as documented by Goldfarb et al. (1991); Goldfarb et al. (1997)

5.3.4 Nitrogen

Similar secular changes of the N isotope composition of mica and K-feldspar from orogenic gold veins and of sedimentary rocks suggest that hydrothermal fluids were dominantly derived from metamorphic dehydration of sedimentary rocks, consistent with the oxygen and hydrogen isotopic composition (Jia and Kerrich 1999, 2004; Jia et al. 2001, 2003), or that were equilibrated with sedimentary rocks along the fluid pathway (Kreuzer 2005). Nitrogen is incorporated into sedimentary rocks by biological activity and is thus mainly bound to organic matter. Organic matter displays a wide range of

$\delta^{15}N$ values (−4–15‰) (Minagawa and Wada 1986; Wu et al. 1997; Gu 2009). Kerogen in sedimentary rocks displays a more limited range of $\delta^{15}N$ values (2–6‰) (Williams et al. 1995; Ader et al. 1998; Sephton et al. 2002), whereas organic N in marine sediments ranges between 0‰ and 10‰ (Peters et al. 1978; Compton et al. 1992; Williams et al. 1995). During diagenesis and metamorphism, the maturation of organic matter releases ammonium (NH_4^+) that substitutes for K^+ in mica and K-feldspar. Metamorphic rocks display $\delta^{15}N$ values between 2 and 17‰ (Haendel et al. 1986; Bebout and Fogel 1992; Jia and Kerrich 2000). Some studies argued that metamorphism decreases the N concentration, and increase $\delta^{15}N$ values of the metamorphosed rocks (Haendel et al. 1986; Bebout and Fogel 1992), but the N isotope fractionation between source rock, hydrothermal fluid and newly formed minerals is small (Busigny et al. 2003; Jia et al. 2003; Jia and Kerrich 2004; Pitcairn et al. 2005; Kerrich et al. 2006).

5.3.5 Boron

The B isotope composition of tourmaline from orogenic gold deposits displays a wide range of values from −22‰ and 9‰ (Fig. 13). At temperatures between 250 and 550 °C, the tourmaline-fluid fractionation ranges from −4.5 and −1.6‰, (Meyer et al. 2008). Consequently, the large variation of 30‰ for $\delta^{11}B$ values cannot be the result of variation in the temperature of formation of orogenic gold deposits. The B isotope composition of the marine seawater reservoir has values near 40‰. In contrast, $\delta^{11}B$ values of others terrestrial reservoirs mostly overlap: continental crust (−6 to −14‰), I-type and S-type magmas (−7 to 3‰ and −7 to −15‰, respectively), MORB and mantle rocks (−8 to −6‰), marine sediments (−14 to −2‰), or marine carbonate (−12 to 26‰) (Fig. 13c) (Palmer and Swihart 1996; van Hinsberg et al. 2011; Lambert-Smith et al. 2016; Marschall et al. 2017; Trumbull and Slack 2018).

At the Paleoproterozoic Palokas gold deposit (Fennoscandian Shield), $\delta^{11}B$ values in the range of −4.5—1.0‰ are interpreted to result from a single magmatic-hydrothermal event (Ranta et al. 2017). In the Paleozoic Passagem de Mariana gold deposit (Brazil), Trumbull et al. (2019) reported $\delta^{11}B$ values between −11.5 and 7.1‰ for orogenic gold veins, and argued in favor to a crustal B source derived from the sedimentary rocks hosting the deposit. A similar hypothesis was discussed by Büttner et al. (2016) and Jiang et al. (2002) to explain the range of $\delta^{11}B$ values (−18.4 to −8.9‰ and −21.4 to −17.8‰, respectively) in Proterozoic gold deposits from the Twangiza-Namoya gold belt (Democratic Republic of Congo) and in the Archean Mount Gibson deposit (Yilgarn Craton), respectively.

The contribution of at least two different sources of B is invoked to explain the wide range of $\delta^{11}B$ recorded in some deposits. At Hira Buddini (India), Krienitz et al. (2008) documented tourmaline with $\delta^{11}B$ values between −4 and 9‰, interpreted to result from mixing between a metamorphic fluid ($\delta^{11}B \sim 0$‰), generated by devolatilization of volcanic rocks, and a magmatic fluid ($\delta^{11}B \sim 10$‰) exsolved from I-type granitic intrusions. A similar interpretation was advanced by Molnár et al. (2016) to explain the wide range of $\delta^{11}B$ values (−24.1 to −9.6‰) in the Archean Hattu schist belt (Finland), where the range in values was interpreted to reflect mixing between a heavy magmatic B with a lighter B reservoir from metamorphic devolatilization of sedimentary rocks.

Tourmaline from orogenic gold quartz-tourmaline veins from the Proterozoic Tapera Grande and Quartzito deposits (Brazil) shows $\delta^{11}B$ values ranging from −15.7 to −5.0‰ (Garda et al. 2009). The wide range of value is interpreted to result from mixing B from multiple sources, derived from volcano-sedimentary rocks (higher $\delta^{11}B$), and from granitic or sedimentary rocks with lower $\delta^{11}B$ values. Similarly, tourmaline from the Proterozoic Bhukia gold deposit (India) has $\delta^{11}B$ values in the range of −12.6 to −9.2‰, that have been interpreted to originate from two fluid sources, a granite-derived hydrothermal and a metapelite-derived metamorphic fluids (Hazarika et al. 2019). Lambert-Smith et al. (2016) also argued that the wide

range of $\delta^{11}B$ values, from 3.5 to 19.8‰, in tourmaline from gold-rich veins in the Loulo mining district (Mali), resulted from mixing marine evaporite with a sedimentary-derived B. In the Val-d'Or district, Beaudoin et al. (2013) and Daver et al. (2020) concluded that tourmaline $\delta^{11}B$ values, between −15.6 and −7.7‰, are a result of mixing of a low $\delta^{11}B$ prograde metamorphic fluids released from sedimentary and/or volcanic rocks with a high $\delta^{11}B$ seawater-derived pore fluid. Trumbull et al. (2020) show a bimodal distribution of the $\delta^{11}B$ values for orogenic gold deposit tourmaline, consistent with two common B reservoirs, sourced from metamorphic/igneous rocks (low $\delta^{11}B$) or from seawater-altered volcano-sedimentary rocks (high $\delta^{11}B$).

In summary, B in orogenic gold deposits generally derived from multiple sources. It is generally accepted that B in orogenic deposits is derived from the devolatilization of volcano-sedimentary and/or sedimentary sequences during metamorphism (Jiang et al. 2002; Krienitz et al. 2008; Garda et al. 2009; Beaudoin et al. 2013; Büttner et al. 2016; Lambert-Smith et al. 2016; Molnár et al. 2016; Hazarika et al. 2019; Trumbull et al. 2019; Daver et al. 2020). The wide range of B isotopic values suggest mixing with other B source(s) that remains matter of debate. B-rich seawater-derived fluid (Beaudoin et al. 2013; Lambert-Smith et al. 2016; Daver et al. 2020) has been proposed as possible source, consistent with the upper crustal fluid identified using oxygen and hydrogen isotopes. B-rich magmatic-derived fluid are also suggested in rare cases (Krienitz et al. 2008; Molnár et al. 2016) but are unlikely to be a common boron reservoir.

5.3.6 Silicon

The silicon isotope composition of quartz is poorly documented in orogenic gold deposits. Only 30 $\delta^{30}Si$ values are compiled (Fig. 14a,b), from the Hemlo (Superior Craton) and the Sawaya'erdun (Tianshan Orogen, China) deposits (Ding et al. 1996; Liu et al. 2007). Natural variation of the $\delta^{30}Si$ values between various terrestrial reservoirs is small (Fig. 14c). Mantle peridotite, granulitic lower continental crust, igneous continental rocks, oceanic crust (MORB + OIB), and sedimentary rocks display overlapping ranges of $\delta^{30}Si$ values between −0.8 and 0‰ (Poitrasson 2017). Only chert-BIFs, and seawater stand out with values between −3.6–5.0‰ and 0.6–4.4‰, respectively (Poitrasson 2017). Silicon does not fractionate significantly during fluid-rock interaction at temperatures above 50 °C (Douthitt 1982; Ding et al. 1988; Geilert et al. 2014; Poitrasson 2017), and thus does not provide information on temperature and processes during quartz precipitation. For orogenic gold systems, $\delta^{30}Si$ is mainly used to discuss the source of silicon by comparing the $\delta^{30}Si$ values of the veins with those of the local country-rocks. Hence, (Liu et al. 2007) argued that the silica ($\delta^{30}Si$ = −0.5–0.5‰) associated with the formation of the Sawaya'erdun orogenic gold deposit was derived from sedimentary ($\delta^{30}Si$ = −0.5–1.9‰) and volcanic ($\delta^{30}Si$ = 0.1‰) country rocks.

6 Conclusions

The stable isotope geochemistry of veins minerals has been widely used to constrain various parameters related to fluid systems involved in the formation of orogenic gold deposits. In this review, we compare and integrate multi-isotopes data from numerous deposits worldwide of various ages and locations to identify global trends shared by most of orogenic gold deposits.

6.1 Temperature

Temperature estimates using quartz-silicate, quartz-carbonate and sulfide-sulfide mineral-pairs display consistent temperature ranges of 360 ± 76 °C (σ = 1, n = 332) with no secular changes, which are in agreement with temperatures expected for deposits formed at temperatures typical for the greenschist to lower amphibolite facies of the country rocks. Quartz-silicate pairs are mostly in isotopic equilibrium, suggesting that retrograde isotopic exchange

between minerals and fluids did not disturb the bulk isotopic composition. In contrast, a significant proportion of quartz-carbonate pairs show isotopic disequilibrium. This could result from quartz and carbonate forming at different times, but later oxygen isotopic exchange of carbonate with a low-temperature fluid is more consistent with the paragenetic sequence of orogenic gold deposits. Sulfide-sulfide mineral-pairs are mostly in isotopic equilibrium.

6.2 Fluid Reservoirs

The oxygen and hydrogen isotope composition of fluids indicate that fluid mixing is a process documented in many orogenic gold deposits. The mixing endmembers are a low T—high δD—low $\delta^{18}O$ upper crustal and a high T—low δD—high $\delta^{18}O$ deep-seated fluid reservoirs.

The nature of the upper crustal fluid is surficial water of various origins having experienced long lived exchange with country rocks. Meteoric water is rarely documented and is commonly related to late infiltration disconnected from the formation of the gold deposits. This is likely the case for most low δD values (< −120‰) documented in OH-bearing mineral and fluid inclusion, mainly from Mesozoic deposits.

The deep-seated fluid endmember is likely metamorphic in origin as attested by hydrogen and oxygen isotope compositions of water plotting mostly in the field for metamorphic water, even if a few data plot in the overlapping field for magmatic and metamorphic waters. The $\delta^{11}B$ values also point a metamorphic source for the fluid that mixed with B-rich seawater-derived fluid, consistent with O–H isotope. The $\delta^{15}N$ values of orogenic gold vein minerals also favor a deep-seated fluid reservoir derived from metamorphic dehydration of sedimentary rocks. The contribution of magmatic water exsolved from magma is documented in some specific cases but is not an essential component for the formation of orogenic gold deposits.

Spatial variations of oxygen and hydrogen isotope compositions of deep-seated fluid between districts indicate variable proportions of igneous and sedimentary rocks in the crustal segment released water during prograde metamorphism. Such provinciality is documented for $\delta^{18}O$ values of quartz between cratons and districts.

Finally, a significant number of high δD values (up to 20‰) for water result of (i) muscovite precipitation during wallrock alteration and (ii) successive phase-separation of water associated to cyclic seismic rupture of fault-veins that displays trends of enrichment in deuterium that fit well the data.

6.2.1 Carbon Isotopes

No secular variations of mineral isotope composition are identified for carbon isotopes ($\delta^{13}C$). The $\delta^{13}C$ values in orogenic gold deposits suggest that CO_2 can be derived from the oxidation of reduced carbon and/or from decarbonation reaction of ∼0‰ inorganic sedimentary rocks during metamorphism, or derived from a deep-seated carbon source such as the mantle. Wide ranges of $\delta^{13}C$ are commonly documented at the deposit scale that suggests a carbon contribution from multiple sources, or that fluid acquired its $\delta^{13}C$ isotopic signature along the fluid pathway through exchange with country rocks.

6.2.2 Sulfur Isotope

$\delta^{34}S$ values of sulfide minerals do not display secular variation or provinciality, but display wide ranges of values. Mixing of sulfur from different reservoirs and/or changes in physico-chemical conditions of the fluid at the site of deposition have been proposed to explain the $\delta^{34}S$ variation in a deposit. Commonly, low $\delta^{34}S$ values are attributed to BSR sulfur from sedimentary rocks, whereas positive $\delta^{34}S$ values are attributed to TSR sulfur or igneous sulfur. Orogenic gold deposits hosted by sedimentary rocks contain sulfur leached from the local country rocks. At the deposit scale, $\delta^{34}S$ values record changes in the oxidation state of the hydrothermal fluid related to redox reactions with country rocks along the fluid pathway or at the site of deposition.

Acknowledgements This research has been made possible by the scientific freedom permitted by Discovery Research Grants of the Natural Science and Engineering Council of Canada. We thank Richard Goldfarb for sharing his unique knowledge of orogenic gold deposits and unpublished data. Lydia Lobato and Kevin Andsell are thanked for providing data. The compilation of the database would not have been possible without the help of Émilie Bédard and Samuël Simard. We are grateful for the constructive comments by referee R.J. Goldfarb and a second anonymous reviewer, and Editor D. Huston, which led to significant improvements to the paper. This work is the Metal Earth contribution MERC-ME-2022-38.

References

Ader M, Boudou J-P, Javoy M, Goffe B, Daniels E (1998) Isotope study on organic nitrogen of Westphalian anthracites from the Western Middle field of Pennsylvania (U.S.A.) and from the Bramsche Massif (Germany). Org Geoch 29:315–323. https://doi.org/10.1016/S0146-6380(98)00072-2

Agangi A, Hofmann A, Eickmann B, Marin-Carbonne J, Reddy SM (2016) An atmospheric source of S in Mesoarchaean structurally-controlled gold mineralisation of the Barberton Greenstone Belt. Precambrian Res 285:10–20. https://doi.org/10.1016/j.precamres.2016.09.004

Apodaca LE (1994) Genesis of lode gold deposits of the Rock Creek area, Nome mining district, Seward Peninsula, Alaska. Unpubished PhD thesis, University of Colorado

Beaudoin G (2011) The stable isotope geochemistry of orogenic gold deposits. In: Barra F, Reich M, Campos E, Tornos F (eds) Proceedings of the eleventh Biennial SGA meeting, Antogfagasta, Chile, pp 556–558

Beaudoin G, Chiaradia M (2016) Fluid mixing in orogenic gold deposits: evidence from the H-O-Sr isotope composition of the Val-d'Or vein field (Abitibi, Canada). Chem Geol 437:7–18. https://doi.org/10.1016/j.chemgeo.2016.05.009

Beaudoin G, Pitre D (2005) Stable isotope geochemistry of the Archean Val-d'Or (Canada) orogenic gold vein field. Miner Deposita 40:59–75. https://doi.org/10.1007/s00126-005-0474-z

Beaudoin G, Therrien R, Savard C (2006) 3D numerical modelling of fluid flow in the Val-d'Or orogenic gold district: major crustal shear zones drain fluids from overpressured vein fields. Miner Deposita 41:82–98. https://doi.org/10.1007/s00126-005-0043-5

Beaudoin G, Rollion-Bard C, Giuliani G (2013) The boron isotope composition of tourmaline from the Val-d'Or orogenic gold deposits, Quebec, Canada. In: Mineral deposit research for a high-tech world 12th SGA Biennial meeting, Proceedings vol 3, pp 1090–1092

Beaudoin G, Therrien P (2009) The updated web stable isotope fractionation calculator. In: Handbook of stable isotope analytical techniques, Volume-II. De Groot, P.A. (ed.). Elsevier: 1120–1122

Bebout GE, Fogel ML (1992) Nitrogen-isotope compositions of metasedimentary rocks in the Catalina Schist, California: implications for metamorphic devolatilization history. Geochim Cosmochim Acta 56:2839–2849. https://doi.org/10.1016/0016-7037(92)90363-N

Bierlein FP, Crowe DE (2000) Phanerozoic orogenic lode gold deposits Rev. Econ Geol 13:103–139

Bierlein FP, Christie AB, Smith PK (2004) A comparison of orogenic gold mineralisation in central Victoria (AUS), western South Island (NZ) and Nova Scotia (CAN): implications for variations in the endowment of Palaeozoic metamorphic terrains. Ore Geol Rev 25:125–168

Billstrom K, Broman C, Jonsson E, Recio C, Boyce AJ, Torssander P (2009) Geochronological, stable isotopes and fluid inclusion constraints for a premetamorphic development of the intrusive-hosted Bjorkdal Au deposit, northern Sweden. Int J Earth Sci 98:1027–1052. https://doi.org/10.1007/s00531-008-0301-8

Böhlke JK, Kistler RW (1986) Rb-Sr, K-Ar, and stable isotope evidence for the ages and sources of fluid components of gold-bearing quartz veins in the northern Sierra Nevada foothills metamorphic belt, California. Econ Geol 81:296–322. https://doi.org/10.2113/gsecongeo.81.2.296

Boer RH, Meyer FM, Robb LJ, Graney JR, Vennemann TW, Kesler SE (1995) Mesothermal-type mineralization in the Sabie-Pilgrim's Rest gold field, South Africa. Econ Geol 90:860–876. https://doi.org/10.2113/gsecongeo.90.4.860

Boiron M-C, Cathelineau M, Banks DA, Fourcade S, Vallance J (2003) Mixing of metamorphic and surficial fluids during the uplift of the Hercynian upper crust: consequences for gold deposition. Chem Geol 194:119–141. https://doi.org/10.1016/S0009-2541(02)00274-7

Busigny V, Cartigny P, Philippot P, Ader M, Javoy M (2003) Massive recycling of nitrogen and other fluid-mobile elements (K, Rb, Cs, H) in a cold slab environment: evidence from HP to UHP oceanic metasediments of the Schistes Lustrés nappe (western Alps, Europe). Earth Planet Sci Lett 215:27–42. https://doi.org/10.1016/S0012-821X(03)00453-9

Büttner SH, Reid W, Glodny J, Wiedenbeck M, Chuwa G, Moloto T, Gucsik A (2016) Fluid sources in the Twangiza-Namoya Gold Belt (Democratic Republic of Congo): evidence from tourmaline and fluid compositions, and from boron and Rb–Sr isotope systematics. Precambrian Res 280:161–178. https://doi.org/10.1016/j.precamres.2016.05.006

Cartigny P, Marty B (2013) Nitrogen isotopes and mantle geodynamics: the emergence of life and the atmosphere–crust–mantle connection. Elements 9:359–366. https://doi.org/10.2113/gselements.9.5.359

Chang Z, Large RR, Maslennikov V (2008) Sulfur isotopes in sediment-hosted orogenic gold deposits: evidence for an early timing and a seawater sulfur source. Geology 36:971–974. https://doi.org/10.1130/G25001A.1

Chen Y-J, Pirajno F, Qi J-P (2008) The Shanggong gold deposit, Eastern Qinling Orogen, China: isotope geochemistry and implications for ore genesis. J Asian Earth Sci 33:252–266

Claypool GE, Holser WT, Kaplan IR, Sakai H, Zak I (1980) The age curves of sulfur and oxygen isotopes in marine sulfate and their mutual interpretation. Chem Geol 28:199–260. https://doi.org/10.1016/0009-2541(80)90047-9

Clayton RN, O'Neil JR, Mayeda TK (1972) Oxygen isotope exchange between quartz and water. J Geophys Res 1896–1977(77):3057–3067. https://doi.org/10.1029/JB077i017p03057

Compton JS, Williams LB, Ferrell RE (1992) Mineralization of organogenic ammonium in the Monterey Formation, Santa Maria and San Joaquin basins, California, USA. Geochim Cosmochim Acta 56:1979–1991. https://doi.org/10.1016/0016-7037(92)90324-C

Couture JF, Pilote P (1993) The geology and alteration patterns of a disseminated, shear zone-hosted mesothermal gold deposit; the Francoeur 3 Deposit, Rouyn-Noranda, Quebec. Econ Geol 88:1664–1684. https://doi.org/10.2113/gsecongeo.88.6.1664

Cox SF (2005) Coupling between deformation, fluid pressures, and fluid flow in ore-producing hydrothermal systems at depth in the crust. Econ Geol 100th Anniv 39–75

Craig H (1961) Isotopic variations in meteoric waters. Science 133:1702. https://doi.org/10.1126/science.133.3465.1702

Craw D, Upton P, Mackenzie DJ (2009) Hydrothermal alteration styles in ancient and modern orogenic gold deposits, New Zealand. NZ J Geol Geophys 52:11–26. https://doi.org/10.1080/00288300909509874

Criss RE, Gregory RT, Taylor HP (1987) Kinetic theory of oxygen isotopic exchange between minerals and water. Geochim Cosmochim Acta 51:1099–1108. https://doi.org/10.1016/0016-7037(87)90203-1

Daver L, Jébrak M, Beaudoin G, Trumbull RB (2020) Three-stage formation of greenstone-hosted orogenic gold deposits in the Val-d'Or mining district, Abitibi, Canada: evidence from pyrite and tourmaline. Ore Geol Rev 120:103449. https://doi.org/10.1016/j.oregeorev.2020.103449

Deng J, Liu X, Wang Q, Pan R (2015) Origin of the Jiaodong-type Xinli gold deposit, Jiaodong Peninsula, China: constraints from fluid inclusion and C-D–O–S–Sr isotope compositions. Ore Geol Rev 65:674–686. https://doi.org/10.1016/j.oregeorev.2014.04.018

Ding TP, Wan DF, Li JC, Jiang SY, Song HB, Li YH, Liu ZJ (1988) The analytical method of silicon isotopes and its geological application. Miner Deposits 7:90–95

Ding T, Jiang S, Wan D, Li Y, Song H, Liu Z, Yao X (1996) Silicon isotope geochemistry. Geological Publishing House, Beijing

Douthitt CB (1982) The geochemistry of the stable isotopes of silicon. Geochim Cosmochim Acta 46:1449–1458. https://doi.org/10.1016/0016-7037(82)90278-2

Dubé B, Gosselin P (2007) Greenstone-hosted quartz-carbonate vein deposits. Geol Assoc Can Mineral Dep Div Spec Publ 5:49–73

Eilu P, Groves DI (2001) Primary alteration and geochemical dispersion haloes of Archaean orogenic gold deposits in the Yilgarn Craton: the pre-weathering scenario. Geochem Explor Environ Anal 1:183. https://doi.org/10.1144/geochem.1.3.183

Eldridge DL, Guo W, Farquhar J (2016) Theoretical estimates of equilibrium sulfur isotope effects in aqueous sulfur systems: highlighting the role of isomers in the sulfite and sulfoxylate systems. Geochim Cosmochim Acta 195:171–200. https://doi.org/10.1016/j.gca.2016.09.021

Faure K (2003) δD values of fluid inclusion water in quartz and calcite ejecta from active geothermal systems: do values reflect those of original hydrothermal water? Econ Geol 98:657–660. https://doi.org/10.2113/gsecongeo.98.3.657

Fedorowich JS, Stauffer MR, Kerrich R (1991) Structural setting and fluid characteristics of the Proterozoic Tartan Lake gold deposit, Trans-Hudson Orogen, northern Manitoba. Econ Geol 86:1434–1467. https://doi.org/10.2113/gsecongeo.86.7.1434

Foley NK, Bethke PM, Rye RO (1989) A reinterpretation of the δD_{H2O} of inclusion fluids in contemporaneous quartz and sphalerite, Creede mining district, Colorado: a generic problem for shallow orebodies? Econ Geol 84:1966–1977

Gaboury D (2013) Does gold in orogenic deposits come from pyrite in deeply buried carbon-rich sediments?: insight from volatiles in fluid inclusions. Geology 41:1207–1210. https://doi.org/10.1130/g34788.1

Garda GM, Trumbull RB, Beljavskis P, Wiedenbeck M (2009) Boron isotope composition of tourmalinite and vein tourmalines associated with gold mineralization, Serra do Itaberaba Group, central Ribeira Belt, SE Brazil. Chem Geol 264:207–220. https://doi.org/10.1016/j.chemgeo.2009.03.013

Geilert S, Vroon PZ, Roerdink DL, Van Cappellen P, van Bergen MJ (2014) Silicon isotope fractionation during abiotic silica precipitation at low temperatures: inferences from flow-through experiments. Geochim Cosmochim Acta 142:95–114. https://doi.org/10.1016/j.gca.2014.07.003

Giletti BJ (1986) Diffusion effects on oxygen isotope temperatures of slowly cooled igneous and metamorphic rocks. Earth Planet Sci Lett 77:218–228. https://doi.org/10.1016/0012-821X(86)90162-7

Goldfarb RJ, Groves DI (2015) Orogenic gold: common or evolving fluid and metal sources through time. Lithos 233:2–26. https://doi.org/10.1016/j.lithos.2015.07.011

Goldfarb RJ, Newberry RJ, Pickthorn WJ, Gent CA (1991) Oxygen, hydrogen, and sulfur isotope studies in the Juneau gold belt, southeastern Alaska; constraints on the origin of hydrothermal fluids. Econ Geol 86:66–80. https://doi.org/10.2113/gsecongeo.86.1.66

Goldfarb RJ, Miller LD, Leach DL, Snee LW (1997) Gold deposits in metamorphic rocks of Alaska. Econ Geol Mon 9:151–190

Goldfarb RJ, Ayuso R, Miller ML, Ebert SW, Marsh EE, Petsel SA, Miller LD, Bradley D, Johnson C, McClelland W (2004) The Late Cretaceous Donlin Creek gold deposit, southwestern Alaska: controls on epizonal ore formation. Econ Geol 99:643–671. https://doi.org/10.2113/99.4.643

Goldfarb RJ, Baker T, Dubé B, Groves DI, Hart CJR, Gosselin P (2005) Distribution, character, and genesis of gold deposits in metamorphic terranes. Econ Geol 100th Anniv Vol, 407–450

Gosselin P, Dubé B (2005) Gold deposits and gold districts of the world. Geol Surv Can Open File 4895

Graham CM, Atkinson J, Harmon RS (1984) Hydrogen isotope fractionation in the system chlorite-water. Nat Environ Res Counc UK Publ Ser D 25:139–140

Graham CM, Viglino JA, Harmon RS (1987) Experimental study of hydrogen-isotope exchange between aluminous chlorite and water and of hydrogen diffusion in chlorite. Am Mineral 72:566–657

Gray DR, Gregory RT, Durney DW (1991) Rock-buffered fluid-rock interaction in deformed quartz-rich turbidite sequences, eastern Australia. J Geophys Res 96 (B12):19681–19704

Groves DI, Goldfarb RJ, Gebre-Mariam M, Hagemann SG, Robert F (1998) Orogenic gold deposits: a proposed classification in the context of their crustal distribution and relationship to other gold deposit types. Ore Geol Rev 13:7–27

Gu B (2009) Variations and controls of nitrogen stable isotopes in particulate organic matter of lakes. Oecologia 160:421–431. https://doi.org/10.1007/s00442-009-1323-z

Haeberlin Y (2002) Geological and structural setting, age, and geochemistry of the orogenic gold deposits at the Pataz Province, eastern Andean Cordillera, Peru. Unpublishe PhD thesis, Université de Genève

Haendel D, Mühle K, Nitzsche H-M, Stiehl G, Wand U (1986) Isotopic variations of the fixed nitrogen in metamorphic rocks. Geochim Cosmochim Acta 50:749–758. https://doi.org/10.1016/0016-7037(86)90351-0

Hagemann SG, Gebre-Mariam M, Groves DI (1994) Surface-water influx in shallow-level Archean lode-gold deposits in Western, Australia. Geology 22:1067–1070. https://doi.org/10.1130/0091-7613(1994)022%3c1067:swiisl%3e2.3.co;2

Hattori K, Cameron EM (1986) Archaean magmatic sulphate. Nature 319:45–47

Hazarika P, Bhuyan N, Upadhyay D, Abhinay K, Singh NN (2019) The nature and sources of ore-forming fluids in the Bhukia gold deposit, Western India: constraints from chemical and boron isotopic composition of tourmaline. Lithos 350–351:105227. https://doi.org/10.1016/j.lithos.2019.105227

Helt KM, Williams-Jones AE, Clark JR, Wing BA, Wares RP (2014) Constraints on the genesis of the Archean oxidized, intrusion-related Canadian Malartic gold deposit, Quebec, Canada. Econ Geol 109:713–735. https://doi.org/10.2113/econgeo.109.3.713

Ho SE, Groves DI, McNaughton NJ, Mikucki EJ (1992) The source of ore fluids and solutes in Archaean lode-gold deposits of Western Australia. J Volcanol Geotherm Res 50:173–196

Horita J, Wesolowski DJ (1994) Liquid-vapor fractionation of oxygen and hydrogen isotopes of water from the freezing to the critical temperature. Geochim Cosmochim Acta 58:3425–3437. https://doi.org/10.1016/0016-7037(94)90096-5

Jia Y, Kerrich R (1999) Nitrogen isotope systematics of mesothermal lode gold deposits: Metamorphic, granitic, meteoric water, or mantle origin? Geology 27:1051–1054. https://doi.org/10.1130/0091-7613(1999)027%3c1051:nisoml%3e2.3.co;2

Jia Y, Kerrich R (2000) Giant quartz vein systems in accretionary orogenic belts: the evidence for a metamorphic fluid origin from $\delta^{15}N$ and $\delta^{13}C$ studies. Earth Planet Sci Lett 184:211–224

Jia Y, Kerrich R (2004) Nitrogen 15–enriched Precambrian kerogen and hydrothermal systems. Geochem Geophys Geosys 5:Q07005. https://doi.org/10.1029/2004GC000716

Jia Y, Li XIA, Kerrich R (2001) Stable Isotope (O, H, S, C, and N) Systematics of quartz vein systems in the turbidite-hosted Central and North Deborah gold deposits of the Bendigo gold field, central Victoria, Australia: constraints on the origin of ore-forming fluids. Econ Geol 96:705–721. https://doi.org/10.2113/96.4.705

Jia Y, Kerrich R, Goldfarb R (2003) Metamorphic origin of ore-forming fluids for orogenic gold-bearing quartz vein systems in the North American Cordillera: constraints from a reconnaissance study of $\delta^{15}N$, δD, and $\delta^{18}O$. Econ Geol 98:109–123. https://doi.org/10.2113/98.1.109

Jiang S-Y, Palmer MR, Yeats CJ (2002) Chemical and boron isotopic compositions of tourmaline from the Archean Big Bell and Mount Gibson gold deposits, Murchison Province, Yilgarn Craton, Western Australia. Chem Geol 188:229–247. https://doi.org/10.1016/s0009-2541(02)00107-9

Johnston DT, Farquhar J, Canfield DE (2007) Sulfur isotope insights into microbial sulfate reduction: When microbes meet models. Geochim Cosmochim Acta 71:3929–3947. https://doi.org/10.1016/j.gca.2007.05.008

Kajiwara Y, Krouse HR (1971) Sulfur isotope partitioning in metallic sulfide systems. Can J Earth Sci 8:1397–1408. https://doi.org/10.1139/e71-129

Kerrich R (1987) The stable isotope geochemistry of Au-Ag vein deposits in metamorphic rocks. Miner Assoc Can Short Course Handb 13:287–336

Kerrich R (1989) Geochemical evidence on the sources of fluids and solutes for shear zone hosted mesothermal gold deposits. Geol Assoc Can Short Course Notes 6:129–198

Kerrich R, Jia Y, Manikyamba C, Naqvi SM (2006) Secular variations of N-isotopes in terrestrial reservoirs and ore deposits. Geol Soc Am Mem 198:81–104

Klein EL, Harris C, Giret A, Moura CAV (2007) The Cipoeiro gold deposit, Gurupi Belt, Brazil: geology, chlorite geochemistry, and stable isotope study. J S Am Earth Sci 23:242–255

Klein EL, Ribeiro JWA, Harris C, Moura CAV, Giret A (2008) Geology and fluid characteristics of the Mina Velha and Mandiocal orebodies and implications for the genesis of the orogenic Chega Tudo gold deposit, Gurupi Belt, Brazil. Econ Geol 103:957–980. https://doi.org/10.2113/gsecongeo.103.5.957

Kontak DJ, Smith PK (1989) Sulphur isotopic composition of sulphides from the Beaver Dam and other Meguma-Group-hosted gold deposits, Nova Scotia; implications for genetic models. Can J Earth Sci 26:1617–1629

Kontak DJ, Kerrich R (1997) An isotopic (C, O, Sr) study of vein gold deposits in the Meguma Terrane, Nova Scotia; implication for source reservoirs. Econ Geol 92:161–180. https://doi.org/10.2113/gsecongeo.92.2.161

Kotzer TG, Kyser TK, King RW, Kerrich R (1993) An empirical oxygen- and hydrogen-isotope geothermometer for quartz-tourmaline and tourmaline-water. Geochim Cosmochim Acta 57:3421–3426. https://doi.org/10.1016/0016-7037(93)90548-B

Kreuzer OP (2005) Intrusion-hosted mineralization in the Charters Towers goldfield, north Queensland: new isotopic and fluid inclusion constraints on the timing and rrigin of the auriferous veins. Econ Geol 100:1583–1603. https://doi.org/10.2113/100.8.1583

Krienitz M, Trumbull R, Hellmann A, Kolb J, Meyer F, Wiedenbeck M (2008) Hydrothermal gold mineralization at the Hira Buddini gold mine, India: constraints on fluid evolution and fluid sources from boron isotopic compositions of tourmaline. Miner Deposita 43:421–434. https://doi.org/10.1007/s00126-007-0172-0

Labidi J, Cartigny P, Moreira M (2013) Non-chondritic sulphur isotope composition of the terrestrial mantle. Nature 501:208–211. https://doi.org/10.1038/nature12490

LaFlamme C, Sugiono D, Thébaud N, Caruso S, Fiorentini M, Selvaraja V, Jeon H, Voute F, Martin L (2018) Multiple sulfur isotopes monitor fluid evolution of an Archean orogenic gold deposit. Geochim Cosmochim Acta 222:436–446. https://doi.org/10.1016/j.gca.2017.11.003

Lambert-Smith JS, Rocholl A, Treloar PJ, Lawrence DM (2016) Discriminating fluid source regions in orogenic gold deposits using B-isotopes. Geochim Cosmochim Acta 194:57–76. https://doi.org/10.1016/j.gca.2016.08.025

Li J-W, Bi S-J, Selby D, Chen L, Vasconcelos P, Thiede D, Zhou M-F, Zhao X-F, Li Z-K, Qiu H-N (2012) Giant Mesozoic gold provinces related to the destruction of the North China craton. Earth Planet Sci Lett 349–350:26–37. https://doi.org/10.1016/j.epsl.2012.06.058

Li Y, Liu J (2006) Calculation of sulfur isotope fractionation in sulfides. Geochim Cosmochim Acta 70:1789–1795. https://doi.org/10.1016/j.gca.2005.12.015

Liu P (1992) The origin of the Archean Jardine iron formation-hosted lode gold deposit, Montana. Unpublished MS thesis, Iowa State University

Liu J, Zheng M, Cook NJ, Long X, Deng J, Zhai Y (2007) Geological and geochemical characteristics of the Sawaya'erdun gold deposit, southwestern Chinese Tianshan. Ore Geol Rev 32:125–156

Liu S, Li Y, Liu J, Shi Y (2015) First-principles study of sulfur isotope fractionation in pyrite-type disulfides. Am Mineral 100:203–208. https://doi.org/10.2138/am-2015-5003

Machel HG, Krouse HR, Sassen R (1995) Products and distinguishing criteria of bacterial and thermochemical sulfate reduction. Appl Geochem 10:373–389. https://doi.org/10.1016/0883-2927(95)00008-8

Madu BE, Nesbitt BE, Muehlenbachs K (1990) A mesothermal gold-stibnite-quartz vein occurrence in the Canadian Cordillera. Econ Geol 85:1260–1268. https://doi.org/10.2113/gsecongeo.85.6.1260

Mao J, Wang Y, Li H, Pirajno F, Zhang C, Wang R (2008) The relationship of mantle-derived fluids to gold metallogenesis in the Jiaodong Peninsula: Evidence from D-O-C-S isotope systematics. Ore Geol Rev 33:361–381

Marschall HR, Wanless VD, Shimizu N, Pogge von Strandmann PAE, Elliott T, Monteleone BD (2017) The boron and lithium isotopic composition of mid-ocean ridge basalts and the mantle. Geochim Cosmochim Acta 207:102–138. https://doi.org/10.1016/j.gca.2017.03.028

McCuaig TC, Kerrich R (1998) P-T-t-deformation-fluid characteristics of lode gold deposits: evidence from alteration systematics. Ore Geol Rev 12:381–453

Meyer C, Wunder B, Meixner A, Romer RL, Heinrich W (2008) Boron-isotope fractionation between tourmaline and fluid: an experimental re-investigation. Contrib Miner Petrol 156:259–267. https://doi.org/10.1007/s00410-008-0285-1

Minagawa M, Wada E (1986) Nitrogen isotope ratios of red tide organisms in the East China Sea: a characterization of biological nitrogen fixation. Mar Chem 19:245–259

Molnár F, Mänttäri I, O'Brien H, Lahaye Y, Pakkanen L, Johanson B, Käpyaho A, Sorjonen-Ward P, Whitehouse M, Sakellaris G (2016) Boron, sulphur and copper isotope systematics in the orogenic gold

deposits of the Archaean Hattu schist belt, eastern Finland. Ore Geol Rev 77:133–162. https://doi.org/10.1016/j.oregeorev.2016.02.012

Nesbitt BE, Muehlenbachs K, Murowchick JB (1987) Comment and reply on "Dual origins of lode gold deposits in the Canadian Cordillera." Geology 15:472–473

Nesbitt BE, Muehlenbachs K, Murowchick JB (1989) Genetic implications of stable isotope characteristics of mesothermal Au deposits and related Sb and Hg deposits in the Canadian Cordillera. Econ Geol 84:1489–1506. https://doi.org/10.2113/gsecongeo.84.6.1489

Neumayr P, Walshe J, Hagemann S, Petersen K, Roache A, Frikken P, Horn L, Halley S (2008) Oxidized and reduced mineral assemblages in greenstone belt rocks of the St. Ives gold camp, Western Australia: vectors to high-grade ore bodies in Archaean gold deposits? Mineral Deposita 43:363–371. https://doi.org/10.1007/s00126-007-0170-2

Nie F-J, Bjorlykke A (1994) Lead and sulfur isotope studies of the Wulashan quartz-K feldspar and quartz vein gold deposit, southwestern Inner Mongolia, People's Republic of China. Econ Geol 89:1289–1305. https://doi.org/10.2113/gsecongeo.89.6.1289

Nie F (1998) Geology and Origin of the Dongping alkalic-type gold deposit, northern Hebei Province, People's Republic of China. Resource Geol 48:139–158. https://doi.org/10.1111/j.1751-3928.1998.tb00013.x

Oberthuer T, Mumm AS, Vetter U, Simon K, Amanor JA (1996) Gold mineralization in the Ashanti Belt of Ghana; genetic constraints of the stable isotope geochemistry. Econ Geol 91:289–301. https://doi.org/10.2113/gsecongeo.91.2.289

Ohmoto H, Rye RO (1979) Isotopes of sulfur and carbon. In: Barnes HL (ed) Geochemistry of hydrothermal ore deposits, 2nd edn. Wiley, New York, pp 509–567

Palmer MR, Swihart GH (1996) Chapter 13. Boron isotope geochemistry: an oveview In: Palmer MR, Swihart (eds), Boron. De Gruyter, Berlin, Boston, pp 709–744

Pandalai HS, Jadhav GN, Mathew B, Panchapakesan V, Raju KK, Patil ML (2003) Dissolution channels in quartz and the role of pressure changes in gold and sulfide deposition in the Archean, greenstone-hosted, Hutti gold deposit, Karnataka, India. Miner Deposita 38:597–624. https://doi.org/10.1007/s00126-002-0345-9

Peters KE, Sweeney RE, Kaplan IR (1978) Correlation of carbon and nitrogen stable isotope ratios in sedimentary organic matter 1. Limnol Oceanogr 23:598–604. https://doi.org/10.4319/lo.1978.23.4.0598

Petrella L, Thébaud N, Laflamme C, Martin L, Occhipinti S, Bigelow J (2020) In-situ sulfur isotopes analysis as an exploration tool for orogenic gold mineralization in the Granites-Tanami Gold Province, Australia: learnings from the Callie deposit. J Geochem Explor 214:106542. https://doi.org/10.1016/j.gexplo.2020.106542

Phillips GN, Evans KA (2004) Role of CO_2 in the formation of gold deposits. Nature 429:860–863. https://doi.org/10.1038/nature02644

Pickthorn WJ, Goldfarb RJ, Leach DL (1987) Comment and reply on "Dual origins of lode gold deposits in the Canadian Cordillera." Geology 15:471–472

Pitcairn IK, Teagle DAH, Kerrich R, Craw D, Brewer TS (2005) The behavior of nitrogen and nitrogen isotopes during metamorphism and mineralization: evidence from the Otago and Alpine Schists, New Zealand. Earth Planet Sci Lett 233:229–246. https://doi.org/10.1016/j.epsl.2005.01.029

Poitrasson F (2017) Silicon isotope geochemistry. Rev Miner Geochem 82:289–344. https://doi.org/10.2138/rmg.2017.82.8

Ranta J-P, Hanski E, Cook N, Lahaye Y (2017) Source of boron in the Palokas gold deposit, northern Finland: evidence from boron isotopes and major element composition of tourmaline. Miner Deposita 52:733–746. https://doi.org/10.1007/s00126-016-0700-x

Ridley JR, Diamond LW (2000) Fluid chemistry of orogenic lode gold deposits and implications for genetic models. Rev Econ Geol 13:141–162

Robert F, Boullier A-M, Firdaous K (1995) Gold-quartz veins in metamorphic terranes and their bearing on the role of fluids in faulting. J Geophys Res Solid Earth 100:12861–12879. https://doi.org/10.1029/95JB00190

Rushton RW, Nesbitt BE, Muehlenbachs K, Mortensen JK (1993) A fluid inclusion and stable isotope study of Au quartz veins in the Klondike District, Yukon Territory, Canada; a section through a mesothermal vein system. Econ Geol 88:647–678. https://doi.org/10.2113/gsecongeo.88.3.647

Rye DM, Rye RO (1974) Homestake Gold Mine, South Dakota; I, Stable isotope studies. Econ Geol 69:293–317. https://doi.org/10.2113/gsecongeo.69.3.293

Santosh M, Nadeau S, Javoy M (1995) Stable isotopic evidence for the involvement of mantle-derived fluids in Wynad gold mineralization, south India. J Geol 103:718–727

Scheffer C, Tarantola A, Vanderhaeghe O, Rigaudier T, Photiades A (2017) CO_2 flow during orogenic gravitational collapse: syntectonic decarbonation and fluid mixing at the ductile-brittle transition (Lavrion, Greece). Chem Geol 450:248–263. https://doi.org/10.1016/j.chemgeo.2016.12.005

Schwarcz HP, Rees CE (1985) Grant 202 Sulphur isotope studies of Archean gold deposits. Ontario Geol Surv Misc Pap 127:151–156

Seal RR II (2006) Sulfur isotope geochemistry of sulfide minerals. Rev Mineral Geochem 61:633–677. https://doi.org/10.2138/rmg.2006.61.12

Selvaraja V, Caruso S, Fiorentini ML, LaFlamme CK, Bui T-H (2017) Atmospheric sulfur in the orogenic gold deposits of the Archean Yilgarn Craton,

Australia. Geology 45:691–694. https://doi.org/10.1130/G39018.1

Sephton MA, Amor K, Franchi IA, Wignall PB, Newton R, Zonneveld J-P (2002) Carbon and nitrogen isotope disturbances and an end-Norian (Late Triassic) extinction event. Geology 30:1119–1122. https://doi.org/10.1130/0091-7613(2002)030%3c1119:CANIDA%3e2.0.CO;2

Sharp ZD, Kirschner DL (1994) Quartz-calcite oxygen isotope thermometry: a calibration based on natural isotopic variations. Geochim Cosmochim Acta 58:4491–4501. https://doi.org/10.1016/0016-7037(94)90350-6

Sharp ZD (2017) Principles of stable isotope geochemistry, 2nd edn. Albuquerque, University of New Mexico. https://digitalrepository.unm.edu/unm_oer/1/

Shaw RP, Morton RD, Gray J, Krouse HR (1991) Origins of metamorphic lode gold deposits: implications of stable isotope data from the central Rocky Mountains, Canada. Mineral Petrol 43:193–209. https://doi.org/10.1007/BF01166891

Shelton KL, So C-S, Chang J-S (1988) Gold-rich mesothermal vein deposits of the Republic of Korea; geochemical studies of the Jungwon gold area. Econ Geol 83:1221–1237. https://doi.org/10.2113/gsecongeo.83.6.1221

Sheppard SMF (1986) Characterization and isotopic variations in natural waters. Rev Mineral 16:165–183

Sibson RH, Robert F, Poulsen KH (1988) High-angle reverse faults, fluid-pressure cycling, and mesothermal gold-quartz deposits. Geology 16:551–555. https://doi.org/10.1130/0091-7613(1988)016%3c0551:HARFFP%3e2.3.CO;2

Smith TJ, Cloke PL, Kesler SE (1984) Geochemistry of fluid inclusions from the McIntyre-Hollinger gold deposit, Timmins, Ontario, Canada. Econ Geol 79:1265–1285. https://doi.org/10.2113/gsecongeo.79.6.1265

Smithson SB, Wenzel F, Ganchin YV, Morozov LB (2000) Seismic results at Kola and KTB deep scientific borehole: velocities, reflections, fluids, and crustal composition. Tectonophysics 329:301–317

So C-S, Yung S-T, Shelton KL, Zhang D-q (2002) Geochemistry of the Youngbogari deposit, Republic of Korea: an unusual mesothermal gold–silver deposit of the Youngdong area. Geochem J 36:155–171

Steed GM, Morris JH (1997) Isotopic evidence for the origins of a Caledonian gold-arsenopyrite-pyrite deposit at Clontibret, Ireland. Trans Inst Mining Metall Sect B Appl Earth Sci B106:109–118

Sun X, Zhang Y, Xiong D, Sun W, Shi G, Zhai W, Wang S (2009) Crust and mantle contributions to gold-forming process at the Daping deposit, Ailaoshan gold belt, Yunnan, China. Ore Geol Rev 36:235–249

Suzuoki T, Epstein S (1976) Hydrogen isotope fractionation between OH-bearing minerals and water. Geochim Cosmochim Acta 40:1229–1240. https://doi.org/10.1016/0016-7037(76)90158-7

Taylor B (1986) Magmatic volatiles; isotopic variation of C, H, and S. Rev Mineral 16:185–225

Thode HG, Ding T, Crocket JH (1991) Sulphur-isotope and elemental geochemistry studies of the Hemlo gold mineralization, Ontario; sources of sulphur and implications for the mineralization process. Can J Earth Sci 28:13–25

Tornos F, Spiro B, Shepherd TJ, Ribera F (1997) Sandstone-hosted gold lodes of the southern West Asturian Leonese Zone (NW Spain): the role of depth in the genesis of the mineralization. Chronique De La Recherche Minière 528:71–86

Trull T, Nadeau S, Pineau F, Polvé M, Javoy M (1993) C-He systematics in hotspot xenoliths: Implications for mantle carbon contents and carbon recycling. Earth Planet Sci Lett 118:43–64. https://doi.org/10.1016/0012-821X(93)90158-6

Trumbull RB, Slack JF (2018) Boron isotopes in the continental crust: granites, pegmatites, Felsic Volcanic Rocks, and Related Ore Deposits. In: Marschall H, Foster G (eds) Boron isotopes: the fifth element. Springer International Publishing, Cham, pp 249–272

Trumbull RB, Garda GM, Xavier RP, Cavalcanti JAD, Codeço MS (2019) Tourmaline in the Passagem de Mariana gold deposit (Brazil) revisited: major-element, trace-element and B-isotope constraints on metallogenesis. Miner Deposita 54:395–414. https://doi.org/10.1007/s00126-018-0819-z

Trumbull RB, Codeço MS, Jiang S-Y, Palmer MR, Slack JF (2020) Boron isotope variations in tourmaline from hydrothermal ore deposits: a review of controlling factors and insights for mineralizing systems. Ore Geol Rev 125:103682

van Hinsberg VJ, Henry DJ, Marschall HR (2011) Tourmaline: an ideal indicator of its host environment. Can Miner 49:1–16. https://doi.org/10.3749/canmin.49.1.1

Vho A, Lanari P, Rubatto D (2019) An internally-consistent database for oxygen isotope fractionation between minerals. J Petrol 60:21012129. https://doi.org/10.1093/petrology/egaa001

Wanless RK, Rw B, Lowdon JA (1960) Sulfur isotope investigation of the gold-quartz deposits of the Yellowknife District [Northwest Territories]. Econ Geol 55:1591–1621. https://doi.org/10.2113/gsecongeo.55.8.1591

Warr O, Giunta T, Onstott TC, Kieft TL, Harris RL, Nisson DM, Lollar BS (2021) The role of low-temperature 18O exchange in the isotopic evolution of deep subsurface fluids. Chem Geol 561:120027. https://doi.org/10.1016/j.chemgeo.2020.120027

Wenner DB, Taylor HP (1971) Temperatures of serpentinization of ultramafic rocks based on O18/O16 fractionation between coexisting serpentine and magnetite. Contrib Mineral Petrol 32:165–185. https://doi.org/10.1007/BF00643332

Wesolowski D, Ohmoto H (1986) Calculated oxygen isotope fractionation factors between water and the

minerals scheelite and powellite. Econ Geol 81:471–477. https://doi.org/10.2113/gsecongeo.81.2.471

Wilkinson JJ, Johnston JD (1996) Pressure fluctuations, phase separation, and gold precipitation during seismic fracture propagation. Geology 24:395–398. https://doi.org/10.1130/0091-7613(1996)024%3c0395:PFPSAG%3e2.3.CO;2

Williams LB, Ferrell RE, Hutcheon I, Bakel AJ, Walsh MM, Krouse HR (1995) Nitrogen isotope geochemistry of organic matter and minerals during diagenesis and hydrocarbon migration. Geochim Cosmochim Acta 59:765–779. https://doi.org/10.1016/0016-7037(95)00005-K

Wortmann UG, Bernasconi SM, Böttcher ME (2001) Hypersulfidic deep biosphere indicates extreme sulfur isotope fractionation during single-step microbial sulfate reduction. Geology 29:647–650. https://doi.org/10.1130/0091-7613(2001)029%3c0647:HDBIES%3e2.0.CO;2

Wu J, Calvert SE, Wong CS (1997) Nitrogen isotope variations in the subarctic northeast Pacific: relationships to nitrate utilization and trophic structure. Deep Sea Res Part I Oceanogr Res Pap 44:287–314. https://doi.org/10.1016/S0967-0637(96)00099-4

Zeng Q, Wang Z, He H, Wang Y, Zhang S, Liu J (2014) Multiple isotope composition (S, Pb, H, O, He, and Ar) and genetic implications for gold deposits in the Jiapigou gold belt, Northeast China. Miner Deposita 49:145–164. https://doi.org/10.1007/s00126-013-0475-2

Zhang X, Nesbitt BE, Muehlenbachs K (1989) Gold mineralization in the Okanagan Valley, southern British Columbia; fluid inclusion and stable isotope studies. Econ Geol 84:410–424. https://doi.org/10.2113/gsecongeo.84.2.410

Zhang J, Chen Y, Zhang F, Li C (2006) Ore fluid geochemistry of the Jinlongshan Carlin-type gold ore belt in Shaanxi Province, China. Chin J Geochem 25:23–31

Zheng Y-F (1992) Oxygen isotope fractionation in wolframite. Eur J Miner 4:1331–1335